Canopy structure explains the relationship between photosynthesis and sun-induced chlorophyll fluorescence in crops

Benjamin Dechant[1], Youngryel Ryu[1]*, Grayson Badgley[2], Yelu Zeng[2], Joseph A. Berry[2], Yongguang Zhang[3], Yves Goulas[4], Zhaohui Li[3], Qian Zhang[3], Minseok Kang[5], Ji Li[3], Ismaël Moya[4]

[1] Department of Landscape Architecture and Rural Systems Engineering, Seoul National University, South Korea

[2] Department of Global Ecology, Carnegie Institution for Science, Stanford, USA

[3] International Institute for Earth System Sciences, Jiangsu Provincial Key Laboratory of Geographic Information Science and Technology, Nanjing University, Nanjing, China

[4] Dynamic Meteorology Laboratory, Ecole Polytechnique, Palaiseau, France

[5] National Center for AgroMeteorology, Seoul, South Korea

* Corresponding author email address: yryu@snu.ac.kr.

Abstract

Remote sensing of far-red sun-induced chlorophyll fluorescence (SIF) has emerged as an important tool for studying gross primary productivity (GPP) at the global scale. However, the relationship between SIF and GPP at the canopy scale lacks a clear mechanistic explanation. This is largely due to the poorly characterized role of the relative contributions from light absorption, leaf physiology and canopy scattering to the variability of the top-of-canopy, observed SIF signal. In particular, the effect of the canopy structure beyond light absorption is that only a fraction (f_{esc}) of the SIF emitted from all leaves in the canopy can escape from the canopy due to the strong scattering of near-infrared radiation. We combined rice, wheat and corn canopy-level in-situ datasets to study how the physiological and structural components of SIF individually relate to GPP. At seasonal time scales, we found that the structural component of SIF, defined as the product of $APAR$ and f_{esc}, explained the relationship of observed SIF to GPP and even outperformed GPP estimation based on observed SIF at two of the three sites investigated. The underlying reason for the strong performance of the structural SIF component, which was estimated as product of the near-infrared reflectance of vegetation (NIR_V) and PAR, was a considerably strong positive correlation (R^2=0.4-0.6) of f_{esc} to the seasonal dynamics of the photosynthetic light use efficiency (LUE_P). In contrast, the physiological component of SIF, obtained by normalizing observed SIF for f_{esc}, improved the relationship to $APAR$ but considerably decreased the correlation to GPP for all three crops. With the partial exception of wheat, the estimated physiological SIF yield was almost entirely uncorrelated to LUE_P both at seasonal and diurnal time scales. Our findings demonstrate the dominant role of canopy structure in the SIF-GPP relationship and highlight the potential for NIR_V-based GPP estimation even at short time scales. Our study unifies previous results and has important implications for large-scale, remote sensing-based GPP estimation.

Submitted to Remote Sensing of Environment

Keywords: sun-induced chlorophyll fluorescence, light use efficiency, photosynthesis, near-infrared reflectance of vegetation, NIRv, escape fraction, canopy scattering, canopy structure

1. Introduction

Far-red sun-induced chlorophyll fluorescence (SIF) is increasingly used as a proxy for gross primary productivity (GPP) at large scales (Ryu et al., 2019). SIF is an optical signal emitted only from chlorophyll a molecules in vegetation and has a well-documented, empirical relationship to estimate GPP at both the site (Sun et al., 2017; Yang et al., 2015; Yongguang Zhang et al., 2016), regional (Guanter et al., 2014; Yongguang Zhang et al., 2018; Yao Zhang et al., 2016), and global scales (Frankenberg et al., 2011; Guanter et al., 2012; Joiner et al., 2011). The precise reason for the SIF-GPP relationship at the canopy scale, however, lacks a clear mechanistic explanation, which is mostly due to an insufficient understanding of the relative contributions of leaf physiological and canopy structure effects to SIF and how the physiological and structural components of SIF relate to photosynthetic light use efficiency. Therefore, it is helpful to revisit the basic processes and equations relevant for SIF and GPP as the basis for more closely examining the possible mechanisms that might underlie their strong empirical correspondence.

SIF and GPP differ in one important respect with regard to their fundamental processes. GPP is related to leaf-level gas exchange processes and therefore, observed top-of-canopy GPP is simply the cumulated GPP of all leaves, as gases that might temporarily accumulate in the canopy eventually will diffuse out of it. SIF, however, is an optical signal in the near-infrared spectral range, where light is strongly scattered by leaves allowing only a certain fraction to escape the canopy (Knyazikhin et al., 2013; Yang and van der Tol, 2018; Zeng et al., 2019). Therefore, the top-of-canopy SIF as observed from tower, airborne or satellite platforms is not simply the cumulative signal of SIF emitted by all leaves but contains an extra term quantifying the effect of canopy scattering. Both SIF and GPP can be understood conceptually in the light use framework originally introduced for net primary productivity (Monteith, 1972; Monteith and Moss, 1977). Thus, for GPP we have

$$GPP = APAR \cdot LUE_P \tag{1}$$

where GPP is defined as the product of the total absorbed photosynthetically active radiation ($APAR$) absorbed by the canopy and the photosynthetic light use efficiency of the canopy (LUE_P). Similarly, for SIF as observed above the canopy (SIF_{obs}), we have

$$SIF_{obs} = APAR \cdot \Phi_F \cdot f_{esc} \tag{2}$$

where Φ_F is the physiological SIF emission yield of the whole canopy and f_{esc} is the fraction of all SIF photons, emitted from all leaves, that escape from the canopy (Zeng et al., 2019). When comparing the basic equations for GPP and SIF, Φ_F corresponds to the LUE_P term and f_{esc} is the extra term that captures the effects of canopy structure.

Modeling studies from as early as 2012 recognized that f_{esc} plays a significant role in controlling the amount of SIF observed at top-of-canopy (Fournier et al., 2012). In terms of functional dependencies, f_{esc} has been shown to respond strongly to changes in both leaf area index (LAI) (Fournier et al., 2012; Yang and van der Tol, 2018) and leaf angle distribution (Du et al., 2017; Migliavacca et al., 2017; Zeng et al., 2019). More generally, it follows from the results of Zeng et al. (2019) that any canopy structure parameter that influences the near-infrared reflectance (e.g. leaf clumping) can have a considerable effect on f_{esc}.

Despite the advances in our theoretical understanding of f_{esc}, little work has gone into understanding what, if any, role f_{esc} has in explaining the SIF-GPP relationship. Instead, the effects of f_{esc} for relating SIF to GPP have largely been ignored in the SIF literature (e.g. Guanter et al., 2014; Wieneke et al., 2016; Yang et al., 2017, 2015). However, a number of more recent studies have reported direct evidence of distorting effects of f_{esc} on the SIF_{obs}-$APAR$ relationship (Du et al., 2017; Liu et al., 2018) and indirect evidence of how f_{esc} affects the SIF_{obs}-GPP relationships using both process-based modelling and observations (Migliavacca et al., 2017). While it is clear from the literature and Eqn. 2 that f_{esc} partially masks the Φ_F signal, there is no decisive conclusion so far whether f_{esc} is helpful or detrimental for GPP estimation. Two apparently opposing views on this question are presented in more detail in the following paragraphs.

Several studies have argued that canopy structure effects on SIF_{obs} should be corrected for the purpose of optimal GPP estimation based on the assumption that Φ_F has a positive relationship to LUE_P (Du et al., 2017; Liu et al., 2018; Yang and van der Tol, 2018). In terms of quantitative evidence, however, such reasoning has been largely based on the improvement of the $APAR$-SIF relationship when accounting for canopy structure (Du et al., 2017; Liu et al., 2018). However, in considering only the SIF-$APAR$ relationship, these studies are insufficient for evaluating the possible role f_{esc} might have in explaining the SIF-GPP relationship. In particular, as GPP estimation has been the ultimate goal of most SIF research, GPP needs to be explicitly considered in the analysis. Logically, an improvement in the $APAR$-SIF relationships could very well go together with a degradation of the SIF-GPP relationship; the better the relationship of SIF to $APAR$, the smaller the variation of the efficiency term $SIF/APAR$ but LUE_P = $GPP/APAR$ actually represents a special case of an efficiency term with considerable variation. Moreover, we are unaware of any experimental studies that explicitly considered the relationship between Φ_F and LUE_P at the canopy scale. Instead, several studies have evaluated the relationship between LUE_P and the joint influence of canopy physiology (Φ_F) and canopy structure (f_{esc}), as obtained by dividing canopy escaping SIF_{obs} by $APAR$ (Eqn. 2; Miao et al., 2018; Wieneke et al., 2016; K. Yang et al., 2018; Yang et al., 2015). Interestingly, the reasoning that Φ_F underlies the SIF-GPP relationship is not well supported by several strands within the existing SIF literature. At the leaf scale, Φ_F is known both to vary less than LUE_P and to be nonlinearly related to LUE_P in light response curves (Gu et al., 2019; van der Tol et al., 2014). Similarly, in situ measurements have shown low seasonal correlation of Φ_F and $\mathrm{LUE_P}$ (Goulas et al., 2017). At the canopy level, these findings are supported by several experimental studies which have shown higher correlation of SIF_{obs} to $APAR$ compared with SIF_{obs} to GPP (Miao et al., 2018; Wieneke et al., 2018; K. Yang et al., 2018).

In contrast to the Φ_F-based reasoning above highlighting the role of leaf physiology, (Badgley et al., 2019, 2017) have argued that it is precisely the canopy structure that explains the SIF_{obs}-GPP relationship. Their reasoning is based on the NIR reflectance of vegetation (NIR_V), a multi-spectral reflectance-based measurement that is strongly linear with both SIF_{obs} and GPP at large spatial and long temporal scales. However, the NIR_V-GPP relationship has so far not been tested with ground-level spectral observations at the shorter time scales that include diurnal variations of both $APAR$ and LUE_P . Nor have previous studies of NIR_V gone beyond documenting the empirical NIR_V-GPPrelationship. The strong connection between the NIR reflectance and f_{esc} (Liu et al., 2018; Yang and van der Tol, 2018; Zeng et al., 2019) hints at potential links between f_{esc} and LUE_P which could be investigated more directly.

Here, we present a series of experiments to test whether f_{esc} distorts the SIF-GPP relationship and should therefore be corrected for, or whether f_{esc} is the main source of relevant information and underlies the observed SIF-GPP relationship. To accomplish this, two important ingredients are needed. The first one is an appropriate method to quantitatively estimate f_{esc} from observations and the second one is an appropriate experimental dataset to apply such an approach.

An important limitation in previous SIF research has been the difficulty of quantifying f_{esc} using observations. However, several recent studies have provided methods to estimate f_{esc} using reflectance in combination with measures of light interception and absorption (Liu et al., 2018; Yang and van der Tol, 2018; Zeng et al., 2019). These methods are theoretically grounded and empirically supported with process-based models of canopy radiative transfer. The newly available formulas for estimating f_{esc}, in particular the approach proposed by Zeng et al. (2019) that is suitable for both sparse and dense canopies, provide a framework for investigating all components of the overall SIF signal, including Φ_F, when $APAR$ and NIR_V data are available.

A second limitation in the progress of SIF research has been the lack of continuous and long-term canopy-level SIF datasets at eddy covariance sites. The shortage of suitable data is partly attributable to the very high-spectral-resolution instruments needed to reliably retrieve SIF (Damm et al., 2011; Guanter et al., 2013; Meroni et al., 2010). Although there have been growing efforts in the community to increase the coverage of continuous SIF observations, few studies have been published, with most of those studies being limited to a partial growing season at a single site (Goulas et al., 2017; Miao et al., 2018; Wieneke et al., 2018; Yang et al., 2017, 2015; K. Yang et al., 2018). This study overcomes the challenge of limited data by combining data from three different research groups at three different crops sites (rice, wheat and corn). The combined dataset includes crops with both C3 and C4 photosynthetic pathways and each dataset covers an entire growing season with i) continuous canopy-level observations of SIF from high-spectral-resolution instruments, ii) reflectance in the visible and near-infrared range, and iii) GPP from eddy covariance .

Our goal in this study is to test the following two opposing hypotheses on the role of f_{esc} for LUE_P estimation:

(H_{phys}) Φ_F contributes relevant information related to LUE_P, while f_{esc} does not and, therefore, the best GPP estimation is based on the product of $APAR$ and Φ_F alone.

(H_{struc}) f_{esc} contributes relevant information related to LUE_P, while Φ_F does not and, therefore, the best GPP estimation is based on the product of $APAR$ and f_{esc} alone.

The above hypotheses represent the two extreme cases that are chosen for the sake of clarity and simplicity, with the recognition that the truth might actually lie somewhere in between. Furthermore, the results are expected to depend on the time scale as canopy structure changes that affect f_{esc}, which mostly occur at the seasonal time scale, while physiological changes that might affect Φ_F occur over the course of individual days as well as over the growing season. Our analysis therefore considers these different time scales.

2. Materials and methods

2.1 Theoretical framework: decomposing SIF and formulating detailed implications of hypotheses

The basic equation for canopy-level SIF_{obs} in terms of its separate mechanistic components was given in the introduction (Eqn. 2). For convenience in later sections, we define LUE_F = $SIF_{obs}/APAR$ as the apparent light use efficiency of SIF in analogy to the definition of photosynthetic light use efficiency, LUE_P = $GPP/APAR$. The escape fraction of whole canopy SiF emissions can be estimated from NIR_v and $fPAR$ following the approach outlined by Zeng et al. (2019):

$$f_{esc} \approx \frac{NIR_V}{fPAR} \tag{3}$$

where NIR_V is the product of NIR reflectance and the NDVI (Badgley et al., 2017). Zeng et al. (2019) demonstrated the good performance of Eqn. 3 with comprehensive radiative transfer simulations as well as supporting evidence from satellite observations. In particular, they showed that f_{esc} derived from NIR_V performs well even for sparsely vegetated canopies and is minimally affected by changes in soil brightness. When $fPAR$, PAR and NIR_V observations are available, in addition to SIF_{obs}, we can combine Eqns. 2 and 3 to calculate the following two SIF-related variables that either contain only $APAR$ and Φ_F or $APAR$ and f_{esc}:

$$SIF_{phys} = APAR \cdot \Phi_F \tag{4}$$

$$SIF_{struc} = APAR \cdot f_{esc} \tag{5}$$

SIF_{phys} is the physiological component of SIF_{obs} and represents the SIF emitted from all leaves within the canopy. SIF_{struc} is the structural component of SIF_{obs} combining the effects of canopy structure on both light absorption and scattering. SIF_{struc} is entirely independent of dynamic leaf physiological properties, only marginally impacted by leaf pigments and strongly dominated by canopy structure characteristics such as leaf angle distribution, clumping and LAI. A visualization of how the definitions in Eqns. 4 and 5 related to the terms of Eqn. 2 is shown in Fig. 1.

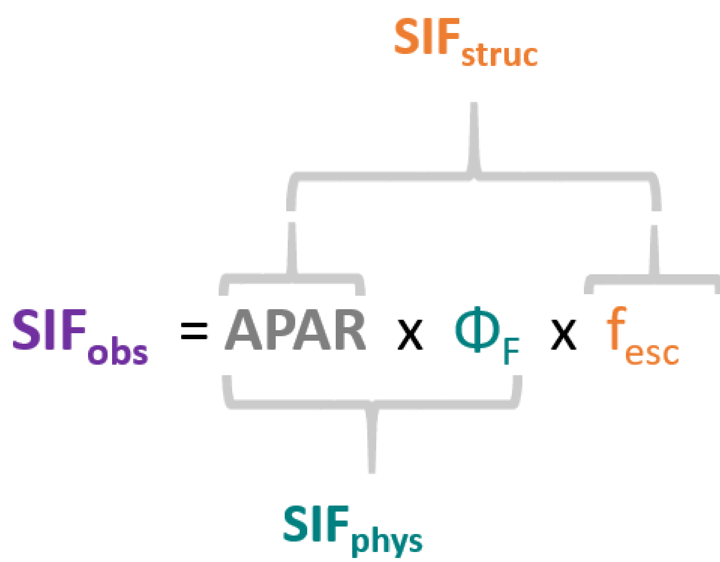

Figure 1: Overview of the conceptual meaning of relevant SIF-related variables. All terms are given at the canopy scale. The light absorption part ($APAR$) is composed of the fraction of absorbed photosynthetically active radiation, $fPAR$, and the level of incoming PAR. Φ_F is the physiological SIF emission yield from all leaves in the canopy and f_{esc} is the fraction of emitted SIF that escapes from the canopy. The canopy escaping, observed SIF ('SIF_{obs}') can be decomposed in the following two ways: first, the product of $APAR$ and Φ_F, which is the total emitted SIF from all leaves in the canopy ('SIF_{phys}') and thus contains the leaf physiological contribution from Φ_F; second, the product of $APAR$ and f_{esc}, which is defined as 'SIF_{struc}' as it represents predominantly the canopy structure contribution. Colours for physiological, structural and combined terms are kept consistently in the presentation of all results for easier visual orientation.

For convenience and clarity we refer to the variables $APAR$, SIF_{struc}, SIF_{phys}, SIF_{obs}, and GPP collectively as 'fluxes', as they all contain an $APAR$ term (Eqns. 1-5) and have units of flux density. Analogously, we refer to the variables f_{esc} , Φ_F, LUE_F and LUE_P collectively as 'efficiencies', given that they are derived from the corresponding flux variables by normalizing for $APAR$ (Eqns. 1, 2, 4, and 5). We conducted all analyses in terms of both fluxes and efficiencies to both cover practically relevant scenarios for GPP estimation (fluxes) and more closely examine underlying mechanisms (efficiencies). All relevant SIF-related variables and their corresponding efficiencies can be derived from Eqns. 1-4 as shown in Table 1. In particular, it is important point out that SIF_{struc} is estimated using only NIR_V and PAR without any contribution from SIF_{obs}.

Table 1: Overview of relevant SIF-related variables and their components in terms of observation or estimation/calculation method and the relevant reference to previous literature or equations in this manuscript. Estimated variables are highlighted with a gray shaded background. PAR is photosynthetically active radiation, $fPAR$ is the fraction of PAR absorbed by the canopy, $APAR$ is the absorbed PAR, SIF_{obs} is the canopy-level observed, far-red sun-induced chlorophyll fluorescence, NIR_V is the near-infrared reflectance of vegetation, NDVI the normalized difference vegetation index, f_{esc} is the fraction of SIF emitted from all leaves in the canopy escaping the canopy, SIF_{phys} is the physiological component of SIF_{obs} and SIF_{phys} is its structural component, Φ_F is the physiological SIF emission yield of the canopy. Obs., calc., and estim. Indicate observed, calculated and estimated, respectively. Canopy reflectance is abbreviated as 'refl.' and the wavelength range over which the average was calculated is indicated in units of nanometer.

variable	obs./calc. /estim.	conceptual meaning/definition	estimation method	reference/eqn. /section
PAR	obs.	-	-	-
$APAR$	obs.	-	-	-
RED	obs.	refl. at 600-650 nm	-	-
NIR	obs.	refl. at 800-850 nm	-	-
SIF_{obs}	obs.	$APAR \cdot \Phi_F \cdot f_{esc}$	-	Eqn. 2
$NDVI$	calc.	$\frac{NIR - RED}{NIR + RED}$	-	Rouse et al. (1973)
NIR_V	calc.	$NDVI \cdot NIR$	-	Badgley, Field and Berry (2017)
$fPAR$	calc.	$PAR/APAR$	-	-
LUE_F	calc.	$SIF_{obs}/ APAR$	-	Eqn. 2, section 2.1.1
f_{esc}	*estim.*	SIF_{obs}/SIF_{phys}	$NIR_V/fPAR$	Eqn. 3, Zeng et al. (2019)
SIF_{struc}	*estim.*	$APAR \cdot f_{esc}$	$NIR_V \cdot PAR$	Eqns. 3, 5
Φ_F	*estim.*	SIF_{obs}/SIF_{struc}	SIF_{obs}/SIF_{struc}	Eqns. 2, 3, 5
SIF_{phys}	*estim.*	$APAR \cdot \Phi_F$	SIF_{obs}/f_{esc}	Eqns. 2, 3, 4

The above decomposition of SIF_{obs} into SIF_{struc} and SIF_{phys} allows us to distinguish six distinct "Cases" that serve as a framework for testing the importance of physiology (H_{phys}) and structure (H_{struc}) in explaining the SIF-GPP relationship. These Cases detail how differences in the correlation of SIF_{obs}, SIF_{struc} and SIF_{phys} to GPP provide evidence to support or refute the two hypotheses, H_{struc} and H_{phys} (Table 2).

H_{phys} would be most strongly supported if SIF_{phys} was a better predictor than SIF_{obs} (Case 1) and SIF_{struc} was a worse predictor of GPP than SIF_{obs} (Case 3). Such a pattern would indicate that f_{esc} indeed obscures the SIF-GPP relationship. In a potential intermediate case, SIF_{phys} could have the same performance as SIF_{obs}, indicating the negligible variability of f_{esc} compared to Φ_F (Case 2). For H_{struc}, three analogous Cases can be formulated that are symmetric to those supporting H_{phys}, i.e. share the same structure but with the roles of f_{esc} and Φ_F and SIF_{phys} and SIF_{struc} exchanged (Cases 4-6 in Table 2).

In addition to considering the SIF-GPP relationship, we also consider how the relationships of SIF_{phys} and SIF_{struc} to $APAR$ differ from those of SIF_{obs}. If Φ_F had a considerable variability, SIF_{phys} should improve over SIF_{obs} in terms of correlation to $APAR$ in all cases and the same holds for f_{esc} and SIF_{struc}. Relating these fluxes to $APAR$ in addition to GPP is instructive in three different respects. First, it helps assessing if either f_{esc} of Φ_F have very small variability. Second, it provides a consistency check in the results if the variability of at least one of these efficiency terms varies considerably. For example, a clear change in GPP estimation performance but no corresponding clear change in $APAR$ estimation performance would be inconsistent. Third, improvements in the $APAR$ estimation performance when using SIF_{phys} (Cases 1 and 6) would amount to evidence of both considerable variability of f_{esc} and the estimation quality, in terms of precision, of f_{esc}. This is not true in the same way for Φ_F, however, as Φ_F is obtained as 'residual' of SIF_{obs} and SIF_{struc} (Table 1, see Sections 4.2 and 4.3).

We used the framework of Table 2 to determine which pair of cases (one for SIF_{struc}, one for SIF_{phys}) best corresponded with observations from the three datasets as a way to assess the validity of the hypotheses H_{struc} and H_{phys}. Finally, we performed all analyses both at seasonal and diurnal time scales to assess potential differences in the results. When discussing the analyses at various time scales, it is convenient to refer to "variability cases" rather than detail temporal resolution (30 min.

vs. daily) and time scale (diurnal vs. seasonal): ‘diurnal variability’ corresponds to analyses of half-hourly data for individual days; ‘diurnal+seasonal variability’ corresponds to half-hourly data at the seasonal time scale; ‘seasonal variability’ corresponds to daily mean values at the seasonal time scale.

Table 2: Overview of the theoretical implications of the two main hypotheses on the estimation performance of gross primary productivity (GPP) and absorbed photosynthetically active radiation ($APAR$) when using either the physiological component of SIF (SIF_{phys}) or the structural component of SIF (SIF_{struc}) as predictors. Upward pointing arrows indicate clear improvement, downward pointing arrows clear degradation and dashes indicate no clear change. The implications in terms of the efficiency terms, namely the escape fraction (f_{esc}) and physiological SIF yield (Φ_F) are also included and a case number is assigned to each row for easier reference in the text. ‘cv(.)’ refers to the coefficient of variation and ‘cor(.)’ to the Pearson correlation function. The upper three rows are shaded in grey to provide a visual guide to the grouping of rows in terms of hypotheses and physiological terms such as SIF_{phys} and H_{phys} are given in normal font while the corresponding structural terms are printed in italic for easier distinguishability. The downward pointing arrows for GPP in cases 3 and 6 are highlighted in bold font to better distinguish them from all other upward pointing arrows.

predictor variable	**GPP estimation performance compared to SIF_{obs}**	**$APAR$ estimation performance compared to SIF_{obs}**	**Implications for efficiency terms**	**Corresponding hypothesis**	**case number**
SIF_{phys}	↑	↑	cor(Φ_F, $\mathrm{LUE_P}$) >> 0 cv(f_{esc})>>0	$\mathrm{H_{phys}}$	1
SIF_{phys}	-	-	$f_{esc} \approx const.$ cv(Φ_F)>>0	$\mathrm{H_{phys}}$	2
SIF_{struc}	**↓**	↑	cor(f_{esc} , $\mathrm{LUE_P}$) ≈ 0 cv(f_{esc})>>0	$\mathrm{H_{phys}}$	3
SIF_{struc}	↑	↑	cor(f_{esc} , $\mathrm{LUE_P}$) >> 0 cv(Φ_F)>>0	H_{struc}	4
SIF_{struc}	-	-	$\Phi_F \approx const.$ cv(f_{esc})>>0	H_{struc}	5
SIF_{phys}	**↓**	↑	cor(Φ_F, $\mathrm{LUE_P}$) ≈ 0 cv(Φ_F)>>0	H_{struc}	6

2.2 In-situ data sets

Three in-situ data sets were combined for the analysis. The data sets differ not only in terms of crop type but also in terms of geographical location, instruments used, observation geometry, and retrieval method used to estimate SIF_{obs}. An overview is given in Table 3 and more detailed descriptions are provided in the following subsections. Half-hourly data from a single growing season for each crop were selected and reduced to periods where SIF_{obs}, canopy reflectance, $APAR$ and GPP observations were all available. Gap-filled GPP data was not used in any of the presented analyses. All sites had in situ observations of $fPAR$. All observations were analyzed at half-hourly time intervals (unless explicitly stated otherwise in the text).

Table 3: Overview of the three field datasets with a focus on SIF observations. For rice, wheat and corn the field of view, sensor height and estimated footprint diameter, SIF retrieval method and spectral resolution (full width at half maximum, FWHM), the acquisition frequency, the number of available half-hourly observations and observation days the geographic location (in units of degrees North and Eat for latitude and longitude, respectively) and the key literature reference are shown. Furthermore the photosynthetic pathway and the values used for flux partitioning ('flux part.') are indicated. In each column, the outlying characteristic is highlighted in bold font. The SIF retrieval methods include the singular vector decomposition (SVD), the spectral fitting method (SFM) and a modified version of the Fraunhofer line depth method (nFLD) as used by Goulas et al. (2017). For the hemispheric field-of-view configuration in the rice paddy, the footprint diameter is given as range from the cumulative 50% to 80% of the total footprint. The cumulative 50% footprint of 20 m diameter also corresponds to the distance of 10 m from the tower with maximum relative contribution. The whole row for wheat is shaded in grey for easier visual distinction between the different rows.

Crop type	Photo-synthetic pathway/ flux part.	Field of view	Obs. height (footprint diameter)	SIF retr. method (FWHM)	Acqui-sition frequency	No. of obs. (30min /days)	Lat. (°N)/ Long. (°E)	Literature Reference
Rice	C3/ night	**Hemi-spheric**	5 m (**20-40 m**)	SVD (0.17 nm)	1/min	**913 /61**	38.2013/ 127.2506	K. Yang et al. (2018)
Wheat	C3/ **day**	Nadir	**20.5 m** (2 m)	nFLD (**0.5 nm**)	**60/min**	620 /47	43.9175/ **4.8797**	Goulas et al. (2017)
Corn	**C4**/ night	Nadir	10 m (4.4 m)	SFM (0.17 nm)	0.5/min	776 /57	34.5199/ 115.5916	Li et al. (2019)

2.2.1 *Rice*

The rice paddy site is located in Cheorwon, South Korea (38.2013°N, 127.2506°E) and is part of the national eddy flux network, KoFlux (Huang et al., 2018). Measurements instruments are operated by Seoul National University and the National Center for Agro Meteorology. An eddy covariance system consisting of a three-dimensional sonic anemometer (Model CSAT3, Campbell Scientific Inc., Logan, UT, USA) and a closed-path infrared gas analyzer (Model LI-7200, LI-COR Inc., Lincoln, NE, USA) was used to measure CO_2 fluxes. Net CO_2 flux partitioning into gross primary production (GPP) and ecosystem respiration was conducted according to the night time-based method (Reichstein et al., 2005). SIF was monitored with a very high spectral resolution instrument (full width at half maximum, FWHM = 0.17 nm, QEpro, Ocean Optics, Dunedin, FL, USA) and a fiber switch to measure up- and downwelling irradiances in sequence (K. Yang et al., 2018; X. Yang et al., 2018). The singular vector decomposition (SVD) method (Guanter et al., 2013) was used for SIF retrieval of data acquired every minute and average over 30 minutes. A fixed integration time was used for all measurements. Canopy reflectance in the visible-near-infrared spectral region (VIS-NIR) was monitored with two lower resolution instruments (FWHM ≈ 4 nm, Jaz, Ocean Optics, Dunedin, FL, USA) which simultaneously observed up- and downwelling radiation fluxes. Both the SIF and canopy reflectance systems were operated in bi-hemispheric field-of-view configurations positioned about 5 m above the rice canopy throughout the whole growing season. This corresponds to an effective footprint size of 40 m diameter when considering the area that contributes 80% of the total signal (Marcolla and Cescatti, 2017). Regular calibration was performed for both SIF and canopy reflectance systems using a calibration light source (HL-2000-Cal, Ocean Optics, Dunedin, FL, USA). $fPAR$ was continuously monitored at three sampling locations using an automated, low-cost observation system based on LED sensors (Kim et al., 2019) but had to be gap-filled with PROSAIL (Jacquemoud et al., 2009; Jacquemoud and Baret, 1990) simulation using observed input data. The data was acquired in the year 2016. A more detailed description of the rice paddy site and the methods used can be found in K. Yang et al. (2018).

2.2.2 *Wheat*

The wheat field is located close to Avignon in southeastern France (43.9175°N, 4.8797°E) and is operated by INRA (‘Institut National de la Recherche Agronomique’). It is also part of CarboEurope

(Dolman et al., 2006) which provided the eddy flux data. The eddy covariance system consists of a three-dimensional sonic anemometer (Model 81000, R.M. Young Company, Traverse City, MI, USA) and an open path infrared gas analyzer (Model LI-7500, LI-COR Inc.). Flux partitioning was done based on day time values (Kowalski et al., 2003). SIF and canopy reflectance was observed with the TriFLEX instrument that consists of separate spectrometers for measurements of SIF and VIS-NIR hyperspectral reflectance (Daumard et al., 2010). The spectrometer for SIF observations has a high spectral resolution (FWHM = 0.5 nm) while the broadband reflectance is observed at lower resolution (FWHM = 2 nm). The TriFLEX instrument was mounted on a crane at 21 m above ground, was operated at nadir observation angle and has a narrow field of view resulting in a footprint diameter of about 2 m (Goulas et al., 2017). In contrast to the system in the rice paddy, downwelling solar irradiance was observed using a white reference panel. SIF was retrieved from high frequency observations (about 1 Hz) using a modified Fraunhofer Line Depth (FLD) method that is described in detail in the corresponding references (Daumard et al., 2010; Goulas et al., 2017) and then averaged over 30 minute periods. $fPAR$ was continuously monitored using a network of ten quantum sensors. The data was acquired in the year 2010. More details on the site and the methods used can be found in Daumard et al. (2010) and Goulas et al. (2017).

2.2.3 Corn

The corn field is located in Henan province, in central China (34.5199° N, 115.5916° E) and is also used for growing winter wheat in a rotation system. The measurement instruments are operated by Nanjing University and the Farmland Irrigation Institute of the Chinese Academy of Agricultural Sciences. An eddy covariance system consisting of a three-dimensional sonic anemometer (WindMaster Pro, Gill Instruments Limited, Hampshire, UK) and a closed path infrared gas analyzer (LI-7500RS, LI-COR Inc., Lincoln, NE, USA) and was continuously operated. Eddy flux partitioning was done according to the night time-based method of Reichstein et al. (2005). A similar system as in the rice paddy based on the FluoSpec2 design (X. Yang et al., 2018; Yang et al., 2015) was used for SIF retrievals (Ocean Optics QEpro spectrometer with FWHM = 0.17 nm). SIF was retrieved from the observations taken every two minutes with a spectral fitting method (SFM) (Meroni et al., 2010; Meroni and Colombo, 2006), before averaging the observations over 30 minute intervals. Integration times were optimized before each measurement. In addition to the high spectral resolution instrument, a lower spectral resolution (FWHM = 1.1 nm) spectrometer covering the VIS-NIR range was used to continuously monitor canopy reflectance changes (HR 2000+, Ocean Optics, Dunedin, FL, USA). The latter was also operated with a shutter system to switch between observations of down- and upwelling radiation. In contrast to the rice paddy observations, the field of view of both spectrometer systems for upwelling observations was 25° as bare fibers were used. As the observations were located about 10 m above the canopy, the measurement footprint circle had a diameter of about 4.4 m (Li et al., 2019). Radiometric calibration was also conducted with the HL-2000-cal light source (Ocean Optics, Dunedin, FL, USA) for downwelling observations and upwelling observations were calibrated by using a white reference panel (Spectralon, Labsphere, NH, USA) at solar noon under clear sky conditions but this was not automated as for the wheat site. $fPAR$ was continuously monitored with one PAR sensor above and four sensors below the canopy. The data was acquired in the year 2017. More details on the site and the methods used can be found in Li et al. (2019).

2.3 Data processing and statistical analysis

For all three crop datasets, only time steps that had valid values for $APAR$, SIF_{obs}, NIR_V and GPP between 8 am and 4 pm were selected in order to ensure comparability of the correlation values for relationships to GPP. For rice and corn, most of the growing season satisfied these criteria, while the wheat site only had data after the green-up phase (supplementary figure Fig. S1). All datasets had some gaps. For all analyses, we further restricted the data by setting a threshold for $fPAR$ above 0.45 in order to exclude the noisy data in the early growing stage. This was only strictly necessary for analyses of efficiency variables but nevertheless also done for flux variables to be consistent.

For the diurnal correlation and daily mean value calculation, only days with a minimum of five valid data points were selected. Combined with the $fPAR$ threshold, this resulted in 61, 47 and 57 days of data for rice, wheat and corn, respectively (Table 3).

SIF_{obs} of the rice dataset was converted from irradiance to radiance units for better comparability with the other two datasets.

NIR_V was calculated from the lower spectral resolution VIS-NIR spectrometers by averaging over the range 800-850 nm for the NIR band and over 600-650 nm for the red band (Table 1). This choice was motivated by the spectral response curves of the corresponding Moderate Imaging Spectrometer (MODIS) bands as either the MODIS satellite data or a similar spectral configuration was used in previous studies (Badgley et al., 2017; Zeng et al., 2019).

All correlation analyses were done based on the Pearson correlation coefficient. Statistical analysis was done using the programming language *R* (R Core Team, 2012).

3. Results

3.1 Relationships between SIF-related variables and GPP or $APAR$

3.1.1 Half-hourly data at seasonal time scale (seasonal + diurnal variability)

There were clear differences in the GPP estimation performance of SIF_{obs}, SIF_{struc}, and SIF_{phys}, with SIF_{struc} having the strongest correlation with GPP (Figs. 2 and 3a). The following pattern of increasing linear correlation to GPP was consistent for all crops: $SIF_{phys} < SIF_{obs} \leq SIF_{struc}$ (Figs. 2 and 3a). SIF_{struc} strictly outperformed SIF_{obs} for rice and corn with R^2 values of 0.75 and 0.82, respectively, but had almost the same performance for wheat with an R^2 of 0.54 and 0.55, respectively. SIF_{phys} had generally much lower correlations to GPP than SIF_{obs} ($0.1<\Delta R^2<0.2$). Overall, differences in R^2 of SIF_{struc} compared to SIF_{obs} were largest for corn, intermediate for rice and smallest for wheat, while the roles of rice and corn were exchanged for the differences between SIF_{phys} and SIF_{struc} (Fig. 3a). While SIF_{struc} showed a slight tendency to saturate at high values in the case of rice and corn, we did not observe this pattern for wheat (Fig. 2d,h,i). Furthermore, the SIF_{obs}-GPP relationship showed clear signs of saturation for corn and wheat but not for rice (Fig. 2c,g,k). For rice and corn, the differences in GPP estimation performance of different SIF predictor variables were mainly caused by deviations from the ideal case of perfect correlation for values in the middle and high part of the GPP range (Fig. 2a-d,i-l). For wheat, however, the deviations from the ideal case was more notable also in the low to middle parts of the GPP range (Fig. 2e-h). Relaxing the $fPAR$ threshold criterion (see section 2.3) did not change the relative GPP estimation performance of SIF_{phys} , SIF_{struc} , and SIF_{obs} and only had marginal effects on the R^2 values for wheat and corn. However, as rice had a prolonged green-up phase resulting in a large number of low GPP values, the performances of predictors for the full dataset without applying the $fPAR$ threshold were considerably higher for all variables ($0.09 \leq \Delta R^2 \leq 0.17$) , in particular SIF_{struc} had an R^2 value of 0.84 (Fig. S2).

For GPP estimation, the performance rank of $APAR$ compared to SIF-related variables differed for wheat, where $APAR$ performed worst, while $SIF_{phys} < APAR < SIF_{obs}$ held for rice and corn (Figs. 2 and 3a). The differences between $APAR$ and SIF_{obs} in terms of absolute increase in R^2 were smallest for corn and largest for wheat. An overview of the time series for all flux variables and crops is given in Fig. S1 in the supplementary material.

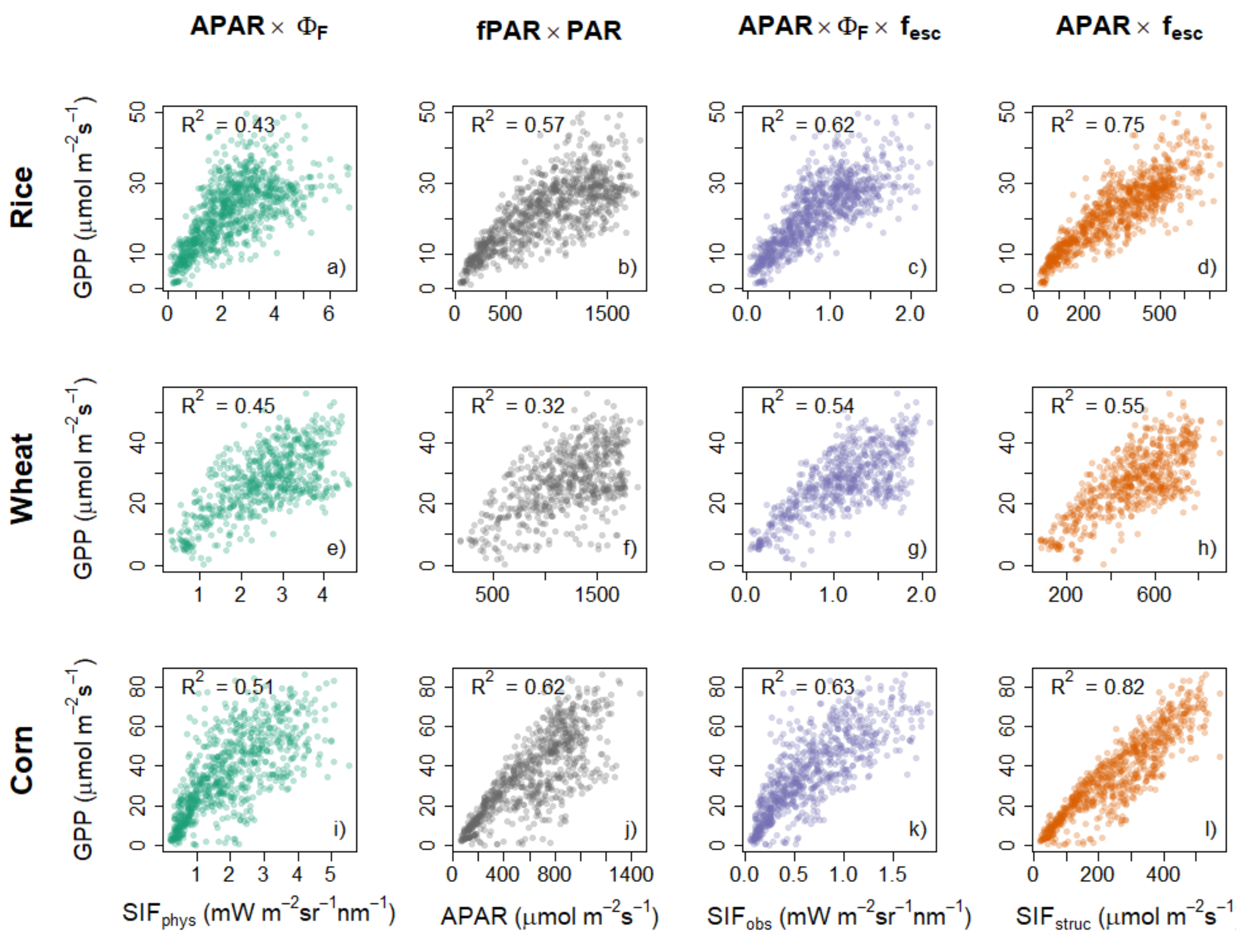

Figure 2: Overview of relationships between gross primary productivity (GPP) and SIF-related variables at half-hourly temporal resolution for the whole growing season (as far as data was available). Absorbed photosynthetically active radiation ($APAR$), and the two other SIF-related variables. GPP is compared with $APAR$ in panels a, e, i, the structural SIF proxy (‘SIF_{struc}’) in panels b, f, j, the physiological SIF proxy (‘SIF_{phys}’) in panels c, g, k, and with observed SIF (‘SIF_{obs}’) in panels d, h, l. The equations for the conceptual definition of all SIF-related variables are shown on top of each column. Relationships are shown on the basis of half-hourly data covering one growing season for each crop. Squared Pearson correlation values (R^2) are shown for reference. All data are shown as partially transparent, filled circles in order to visualize the density of points.

When considering relationships to $APAR$ rather than GPP, both SIF_{struc} and SIF_{phys} had a stronger correlation to $APAR$ than SIF_{obs} (Fig. 3b and Fig. A1 in the appendix). For SIF_{phys}, the improvement was largest for wheat, intermediate for corn and smallest for rice ($0.07 \leq \Delta R^2 \leq 0.19$; Fig. 3b). For SIF_{struc}, the improvement in relationships to $APAR$ was on a similar level for rice and wheat and somewhat larger for corn ($0.11 \leq \Delta R^2 \leq 0.17$ when considering all three crops). Overall, the relationship between SIF_{obs} and $APAR$ was strongest in rice, weaker in corn, and weakest in wheat (0.59≤R^2≤0.73). While this pattern was mostly conserved when using SIF_{struc} (Fig. 3b), SIF_{phys} had a more consistent level of correlation to $APAR$ for all three crops (Fig. 3b). A more detailed analysis of the relationships between $APAR$ and either SIF_{obs}, SIF_{struc} or SIF_{phys} in terms of patterns in the half-hourly scatter plots is presented in Appendix A.

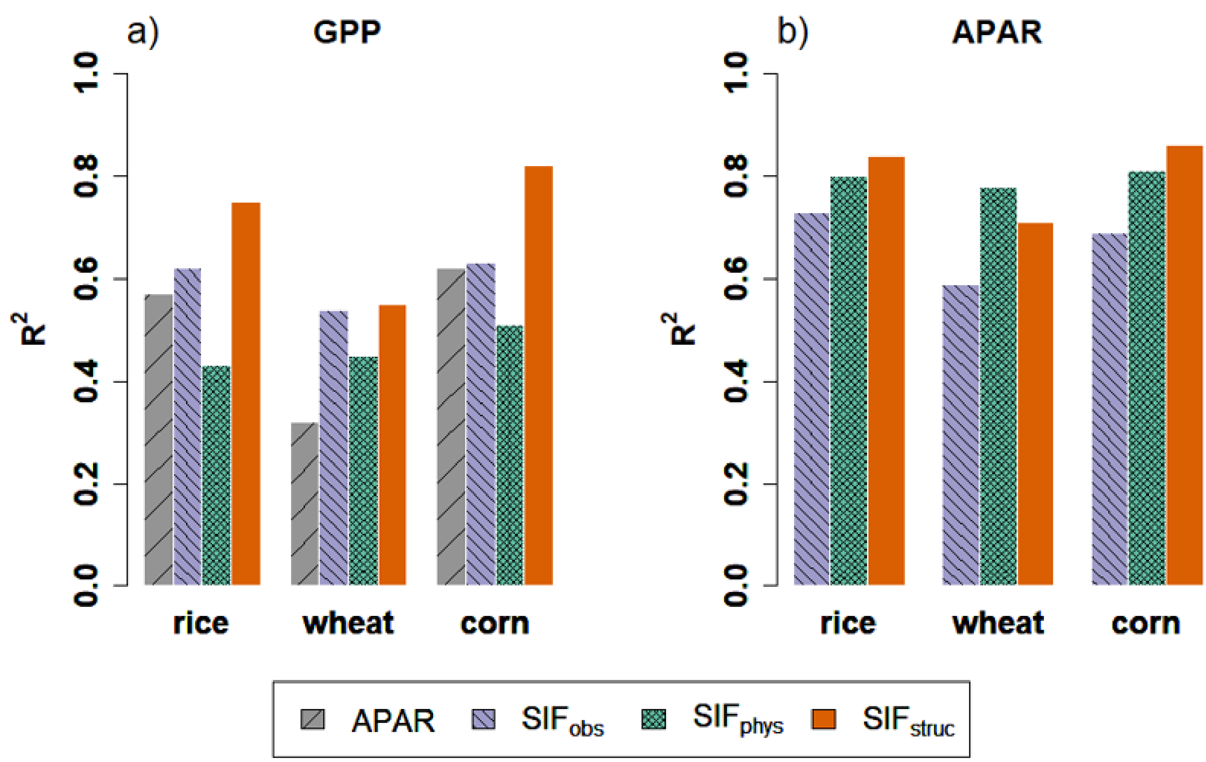

Figure 3: Overview of estimation performance of gross primary productivity (GPP) and absorbed photosynthetically active radiation (APAR) based on different SIF-related predictor variables. Results are shown for half-hourly values at the seasonal time scale. Squared Pearson correlation coefficient values are given per crop and predictor variable. The SIF-related predictor variables other than SIF_{obs} are the physiological SIF ($SIF_{phys} = APAR \cdot f_{esc}$) and the structural SIF proxy ($SIF_{struc} = APAR \cdot \Phi_F$).

3.1.2 Effect of time scale and temporal resolution (seasonal vs. diurnal variability)

The above analysis focused on the combined seasonal and diurnal variability case but as different mechanisms dominate the long (seasonal) and short (diurnal) time scales, it is instructive to separate the diurnal and seasonal variabilities (see sections 2.1 and 2.3 for the methodical descriptions). Following the framework presented in Table 2, we focus on the R^2 differences of either SIF_{phys} compared to SIF_{obs} or SIF_{struc} compared to SIF_{obs} for estimating GPP or $APAR$.

For SIF_{phys} as a GPP predictor, we found small, positive R^2 differences when evaluating for diurnal variability ($0<\Delta R^2<0.03$), and considerable negative values ($\Delta R^2< -0.09$) for both combined diurnal+seasonal variability and seasonal variability (Fig. 4a). The R^2 differences were largest for the seasonal variability (minimum ΔR^2 for rice: -0.28). For $APAR$ estimation, all R^2 differences were positive and there were clearer differences at the diurnal time scale ($0.03<\Delta R^2<0.1$), intermediate values for seasonal+diurnal variability, and, with the exception of corn, the largest values of ΔR^2 for seasonal variability ($0.1\leq\Delta R^2\leq0.22$). R^2 differences of rice and corn showed more similar magnitudes of ΔR^2 values for the seasonal variability cases compared to the larger values of wheat (Fig. 4b).

For SIF_{struc} as GPP predictor, we found that R^2 differences for rice and corn had considerable positive values for all variability cases ($0.07\leq\Delta R^2\leq0.25$), while the values for wheat were very close to zero (<0.02 in terms of absolute values) and slightly negative in two out of the three variability cases (Fig. 4c). Rice showed increasing R^2 differences from diurnal to seasonal time scales, while corn showed the opposite pattern. For $APAR$ estimation, SIF_{struc} had only positive values ($0.04\leq\Delta R^2\leq0.20$) and different patterns for variability cases for each crop (Fig. 4d). The highest R^2 difference was observed for the diurnal case in corn. Rice showed similar levels or R^2 values for all variability cases, while wheat showed a notably smaller values for seasonal variability compared to cases including diurnal variability. Corn showed a decreasing pattern from diurnal to seasonal variability (Fig. 4d), similar to the pattern of GPP estimation (Fig. 4c).

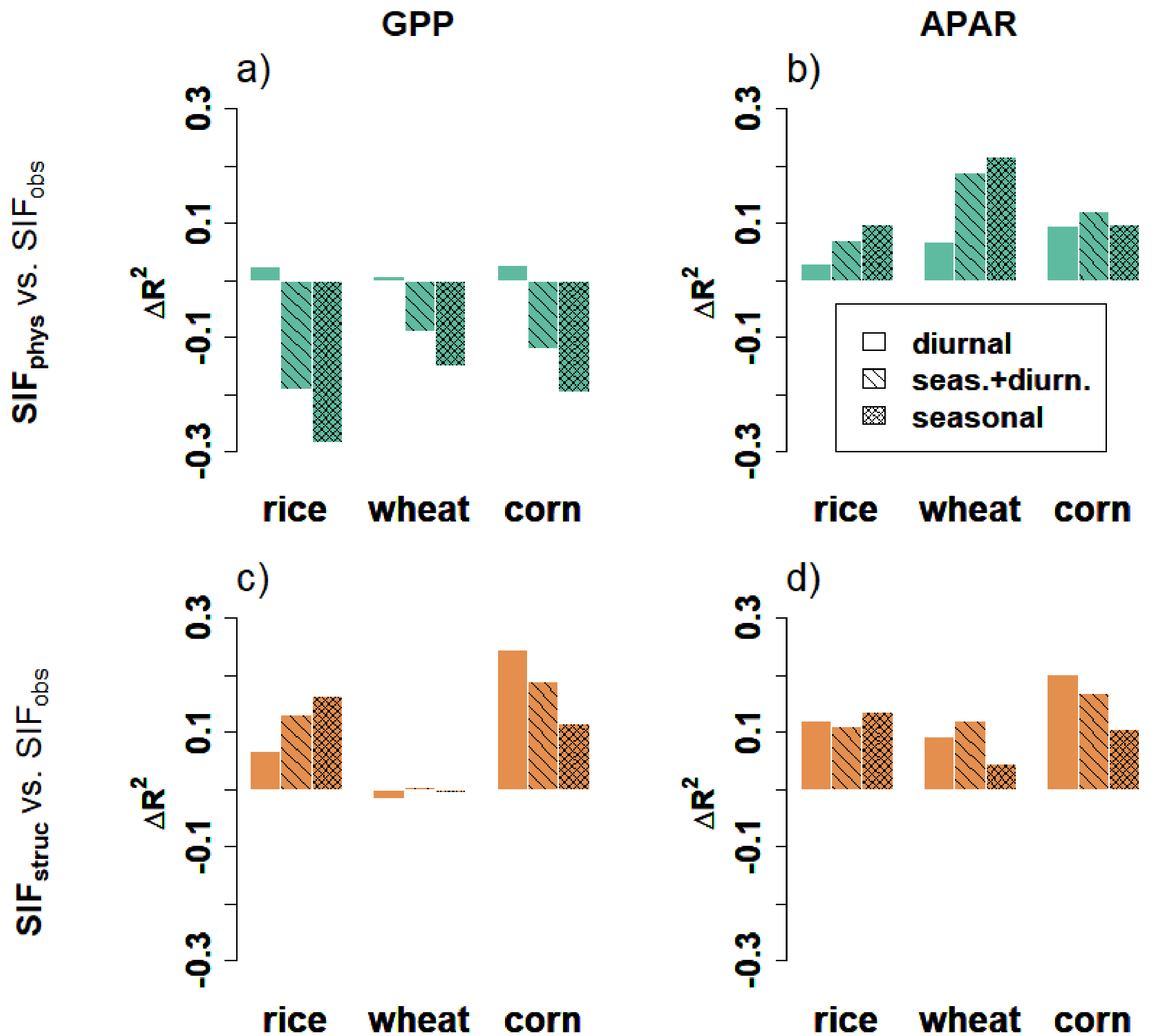

Figure 4: Overview of difference in gross primary productivity ('GPP') estimation performance between either the physiological SIF ($SIF_{phys} = APAR \cdot f_{esc}$) and observed SIF ('$SIF_{obs}$') or the structural SIF proxy ($SIF_{struc} = APAR \cdot \Phi_F$) and SIF_{obs}. Differences in squared Pearson correlation coefficient values (ΔR^2) are given per crop and per variability case. The latter include seasonal variability ('seas.') based on daily mean values, seasonal + diurnal variability ('seas.+diurn') based on half-hourly values at the seasonal time scale and diurnal variability ('diurn.') based on half-hourly values at the diurnal time scale. For the latter, the median values of diurnal correlation of all days (with sufficient data) are shown. The results correspond to those in Fig. 3 in terms of presentation but include the variability separation in terms of time scale and focus on relative patterns rather than absolute values.

3.2 Efficiency variables f_{esc}, Φ_F, LUE_F and $\mathrm{LUE_P}$: temporal patterns and relationships

To this point, our analysis has primarily concerned the absolute, empirical performance of the flux variables SIF_{obs}, SIF_{phys}, and SIF_{struc} in terms of explaining variations in $APAR$ and GPP. We now turn our attention to specifically exploring the underlying efficiency terms, LUE_F, Φ_F and f_{esc} , and how they relate to $\mathrm{LUE_P}$. Such an analysis directly tests the hypotheses H_{struc} and H_{phys} and offers a way to explore the mechanistic processes governing the empirical SIFobs- GPP relationship (Table 2). The focus of our analysis will be on f_{esc} , Φ_F, and $\mathrm{LUE_P}$ as we established already in section 3.1 that SIF_{obs} was always intermediate between SIF_{phys} and SIF_{struc} and, hence, it is clear that LUE_F will mostly have results intermediate to those of f_{esc} and Φ_F.

3.2.1 Temporal patterns

We found clear differences in both the seasonal patterns and the degree of diurnal variability between efficiency variables (Fig. 5). $fPAR$, f_{esc} and LUE_F all appeared to be mainly characterized by considerable seasonal variation (Figs. 5 and S2). $\mathrm{LUE_P}$ and Φ_F, however, showed considerable diurnal variability. In case of LUE_P, the diurnal variation was superposed to the seasonal changes, while for Φ_F it seemed to be the main source of variation.

Despite some apparent general patterns for each variable, we found considerable differences between crops. Patterns of $fPAR$ increase during green-up and decrease during senescence were similar for rice and corn while for wheat, where the data for the green-up phase were not available, $fPAR$ was consistently high. For rice and wheat, $fPAR$ reached maximum values of almost 0.9, while for corn the highest values were around 0.8. Overall, wheat had the lowest diurnal variations for $fPAR$, corn the strongest variations for some of the days and rice an intermediate level of variability. f_{esc} of rice showed the strongest increase during green-up and a moderate decreases during senescence; wheat showed only moderate increase during green-up but strong decrease during senescence and in addition showed a small peak around the day of year 130, which was a cloudy period with considerably lower PAR values (results not shown but see Fig. 6a in Goulas et al., 2017); corn showed only decreasing patterns with a flattening during senescence. Maximum values for f_{esc} were in around 0.5-0.6 for all crops and minimum values were in the range of 0-0.1. As already mentioned above, Φ_F was seasonally rather constant but wheat showed a clear decrease late in the senescence stage that coincided with a decrease in chlorophyll content (Goulas et al., 2017). For corn, a slight decrease followed by an increase late in the season were observed, while for rice, slight decreases appeared during both the late green-up and senescence. LUE_F overall had similar seasonal patterns as f_{esc} but also showed some smaller seasonal patterns similar to Φ_F in addition to more diurnal variability from the latter (results not shown). The seasonal patterns for $\mathrm{LUE_P}$ were partly masked by strong diurnal variations but decreases during senescence could be observed for all three crops (Fig. 5j-l). While the decreasing patterns of LUE_P for wheat and corn were similar and showed relatively steep slopes, the decrease in rice occurred at an earlier stage and after that $\mathrm{LUE_P}$ was rather stable. Increases in LUE_P during green-up were only clearly evident in the case of rice and to a lesser degree for wheat.

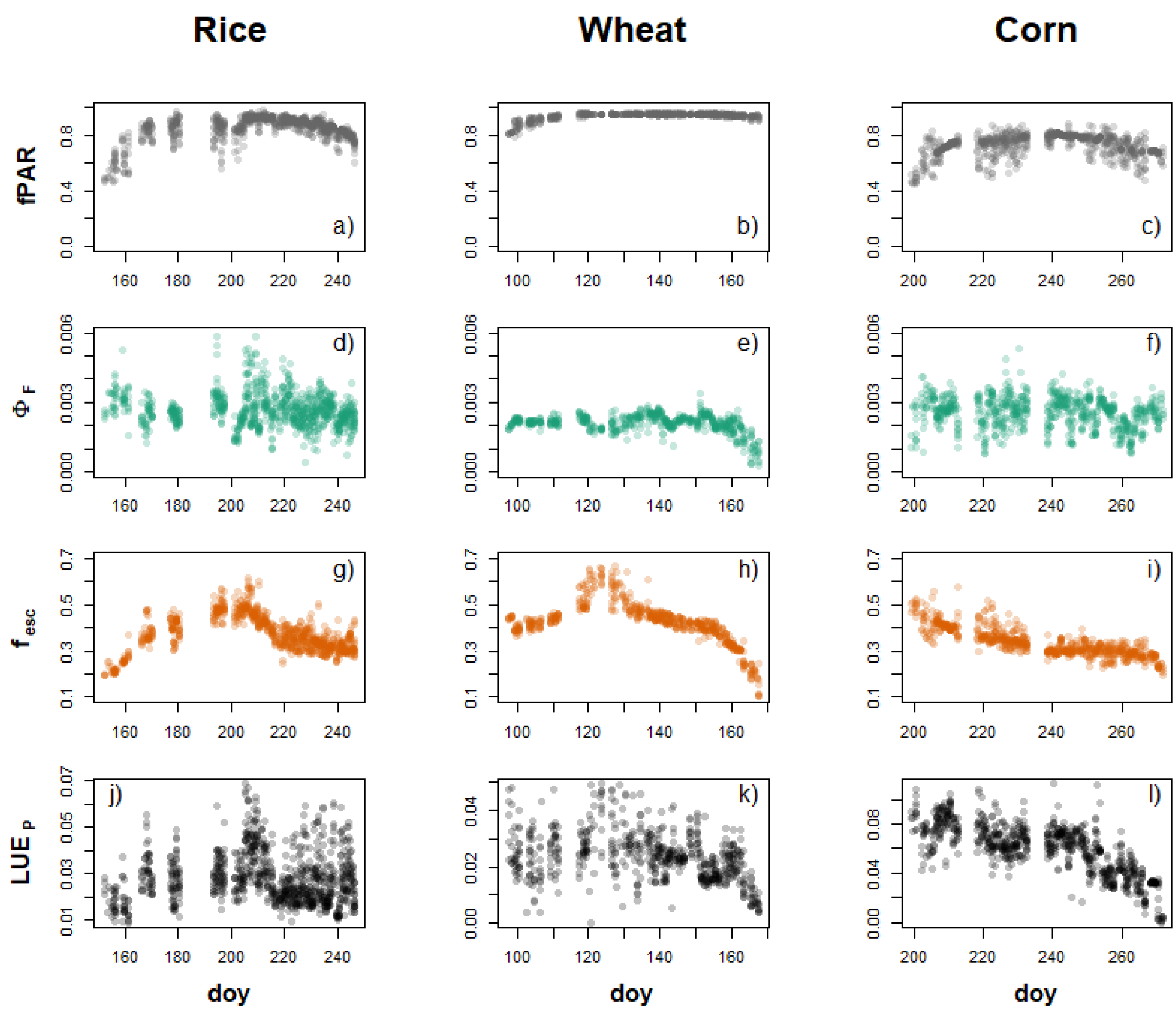

Figure 5: Time series overview of (a-c) fraction of absorbed photosynthetically active radiation ($fPAR$), (d-f) physiological SIF yield (Φ_F), (g-i) escape fraction (f_{esc}), and (j-l) photosynthetic light use efficiency (LUE_P). Half-hourly data are shown as

partially transparent, filled circles in order to visualize the density of data points. Time is shown as day of year (doy). While $fPAR$ and f_{esc} are unitless quantities, LUE_P is shown in units of μmol CO_2 m^{-2} s^{-1}, and Φ_F in units of (mW m^{-2} sr^{-1} nm^{-1})/(μmol photons m^{-2} s^{-1}).

The figure corresponding to Fig. 5 in terms of daily mean values highlighting only the seasonal component of variation and including LUE_F is shown in the supplementary material (Fig. S3).

3.2.2 Relationships to LUE_P

To more directly test our two hypotheses, we built on the qualitative analysis of temporal patterns shown in Fig. 5, by quantifying the correlations of Φ_F and f_{esc} to LUE_P.

In the relationships to $\mathrm{LUE_P}$, the following pattern of increasing performance was consistent for all crops and for seasonal+diurnal variability: Φ_F < LUE_F < f_{esc} (Figs. 6 and S4). Φ_F had R^2 values to LUE_P of zero for both rice and corn and only was slightly higher for wheat (0.08). f_{esc}, in contrast, had values of 0.28, 0.30 and 0.44 for rice, wheat and corn, respectively. The corresponding values for LUE_F were generally on the order of half the value of f_{esc} (Fig. S4). Overall, LUE_F was most strongly related to Φ_F but wheat was an exception where the correlation of f_{esc} was stronger (Fig. S4). f_{esc} and Φ_F were almost entirely unrelated with the only exception in wheat (R^2 = 0.21). For the sake of completeness, we included full correlation tables between all four efficiency terms in the supplementary material (Fig. S4).

When considering the correlations of f_{esc} and Φ_F to LUE_P for diurnal and seasonal variability separately, we found that f_{esc} outperformed Φ_F in all cases but with considerably larger differences for the seasonal variability (Fig. 7a,b). While correlations between Φ_F and LUE_P did not increase much for the seasonal variability compared to the seasonal+diurnal variability for rice and corn and for wheat only moderately (seasonal R^2 = 0.28), the corresponding f_{esc} -LUE_P correlations strongly increased up to 0.6 for wheat and corn and 0.4 for rice (Fig. 7a, b).

The correlations to LUE_P for diurnal variability only showed different patterns compared to the seasonal variability for Φ_F and f_{esc}. For Φ_F, the correlations based on diurnal variability exceeded the R^2 values that included seasonal variability except for wheat where the diurnal value was intermediate between the seasonal+diurnal and the seasonal value (Fig. 7a). For f_{esc}, the diurnal correlations were consistently and considerably lower than those for seasonal+diurnal variability and seasonal variability, although the differences were smaller for rice (Fig. 7b).

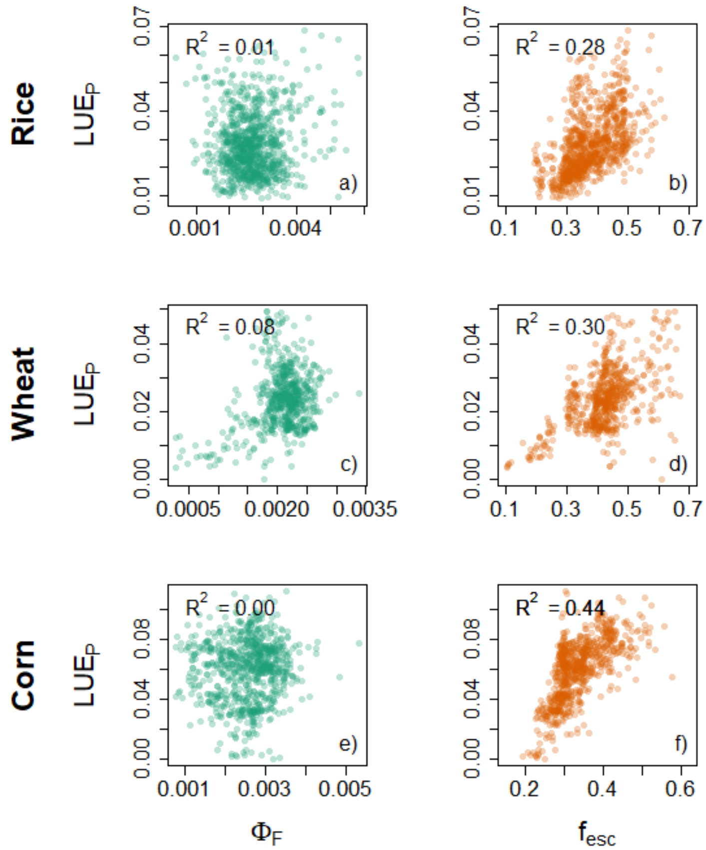

Figure 6: Overview of relationships of physiological SIF yield (Φ_F) and the escape fraction (f_{esc}) to photosynthetic light use efficiency (LUE_P). Results based on either half-hourly or daily mean values at the seasonal scale. For all results, only data for which the fraction of absorbed photosynthetically active radiation, $fPAR$, was larger than 0.45 was selected. Half-hourly data points are shown with partially transparent filled circles in order to indicate point density and corresponding R^2 values are shown. LUE_P is shown in units of µmol CO_2 m^{-2} s^{-1}, and Φ_F in units of (mW m^{-2} nm^{-1} sr^{-1})/(µmol photons m^{-2} s^{-1}).

The diurnal variability case was the only one where LUE_F was not consistently intermediate between Φ_F and f_{esc}. For wheat, LUE_F was slightly more strongly related to LUE_P than either Φ_F or f_{esc} separately and for rice, LUE_F had a slightly lower correlation to LUE_P than Φ_F (Fig. S5b).

In terms of the variability as captured by the CV, Φ_F and f_{esc} showed party consistent patterns. f_{esc} had similar CV values around 0.2 for the seasonal+diurnal and seasonal case but notably smaller values for the diurnal case (CV ≤ 0.07; Fig. 7d). Φ_F also had similar values around 0.2 for the seasonal+diurnal and seasonal case for wheat and the seasonal case of rice and corn but somewhat higher values for the seasonal+diurnal case of rice and corn (Fig. 7c). Diurnal CV value for rice and corn were only slightly smaller than the corresponding seasonal values (around 0.15) but wheat had a considerably smaller diurnal CV (0.06; Fig. 7c). LUE_F and LUE_P showed notably higher CV values (0.3-0.4) than f_{esc} and Φ_F for the seasonal cases (Fig. S5e,g). LUE_F had considerably smaller diurnal CV values than for the seasonal cases, while LUE_P had diurnal values as high almost as the seasonal values except for corn with a much lower diurnal CV (Fig. S5e,g).

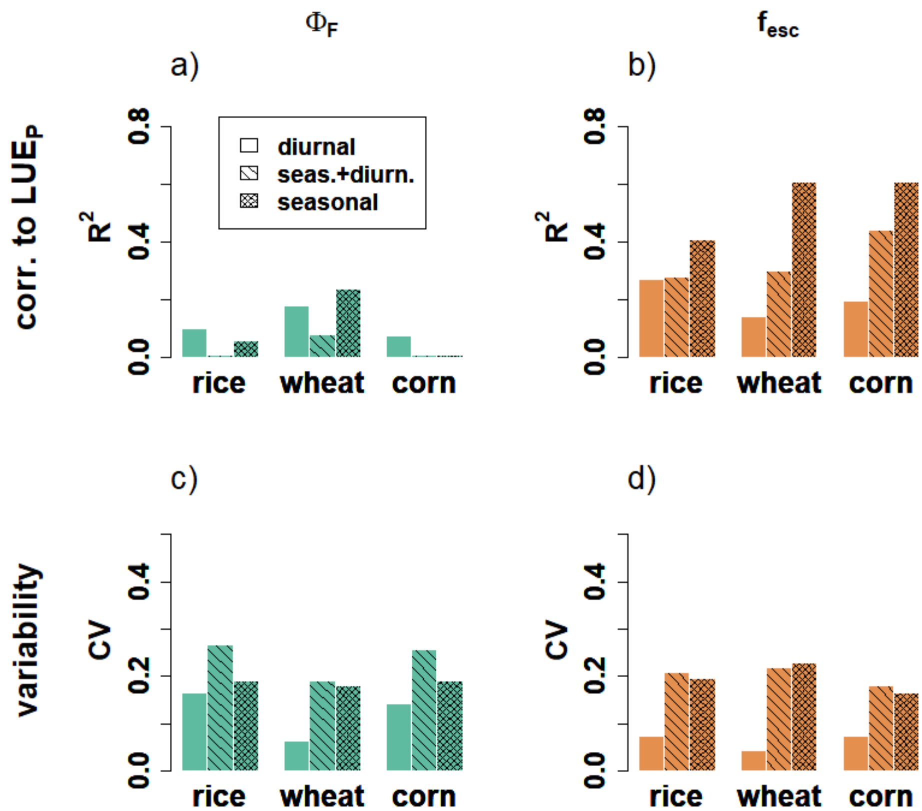

Figure 7: Overview of effects of differences between diurnal and seasonal variability. a),b) effects of variability on the correlation to photosynthetic light use efficiency (LUE_P) and variabilities of c) the physiological SIF yield (Φ_F) d) the escape fraction (f_{esc}). Squared Pearson correlation coefficients (R^2) or coefficients of variation (CV) are shown for each crop and combination of temporal resolution and time scale: seasonal variability based on daily mean values, seasonal + diurnal variability based on half-hourly data at the seasonal time scale and diurnal variability based on the median diurnal R^2/CV at half-hourly temporal resolution.

4. Discussion

4.1 Hypothesis evaluation

In this study, we comprehensively investigated the relationships between SIF and GPP by decomposing observed SIF (SIF_{obs}) into its structural component, SIF_{struc}, and its physiological component, SIF_{phys} (Fig. 1, Table 1). This decomposition allowed us to directly examine the mechanistic basis of the SIF-GPP relationship by studying the underlying relationships of f_{esc} and Φ_F to LUE_P. Relationships of SIF_{obs}, SIF_{phys} and SIF_{struc} to $APAR$ were also studied for comparison.

Overall, we found strong support for the hypothesis H_{struc}, which states that canopy structure, as captured by the escape fraction (f_{esc}), underlies the observed SIF_{obs}-GPP relationship (Fig. 8, Table 4). Moreover, we found that GPP estimation based on SIF_{struc} performed considerably better than or equally well as SIF_{obs} (see Section 4.2 for a more detailed discussion and the link to NIR_V). These findings held consistently at seasonal time scales for the rice and corn datasets and to a lesser degree for the wheat dataset. Even though for wheat data H_{struc} was not strictly fulfilled, the correlation of f_{esc} to LUE_P was considerably stronger than the correlation of Φ_F to LUE_P (Fig. 7a,b). We did not find any results directly supporting the hypothesis H_{phys}, which states that Φ_F carries the more relevant information for GPP estimation and that f_{esc} is a distorting factor (Table 8). However, the results based on the diurnal variability, especially for wheat, indicated that H_{struc} may not hold, in the strictest sense, at the diurnal time scale.

The correlations to LUE_P for diurnal variability only showed different patterns compared to the seasonal variability for Φ_F and f_{esc}. For Φ_F, the correlations based on diurnal variability exceeded the R^2 values that included seasonal variability except for wheat where the diurnal value was intermediate between the seasonal+diurnal and the seasonal value (Fig. 7a). For f_{esc}, the diurnal correlations were consistently and considerably lower than those for seasonal+diurnal variability and seasonal variability, although the differences were smaller for rice (Fig. 7b).

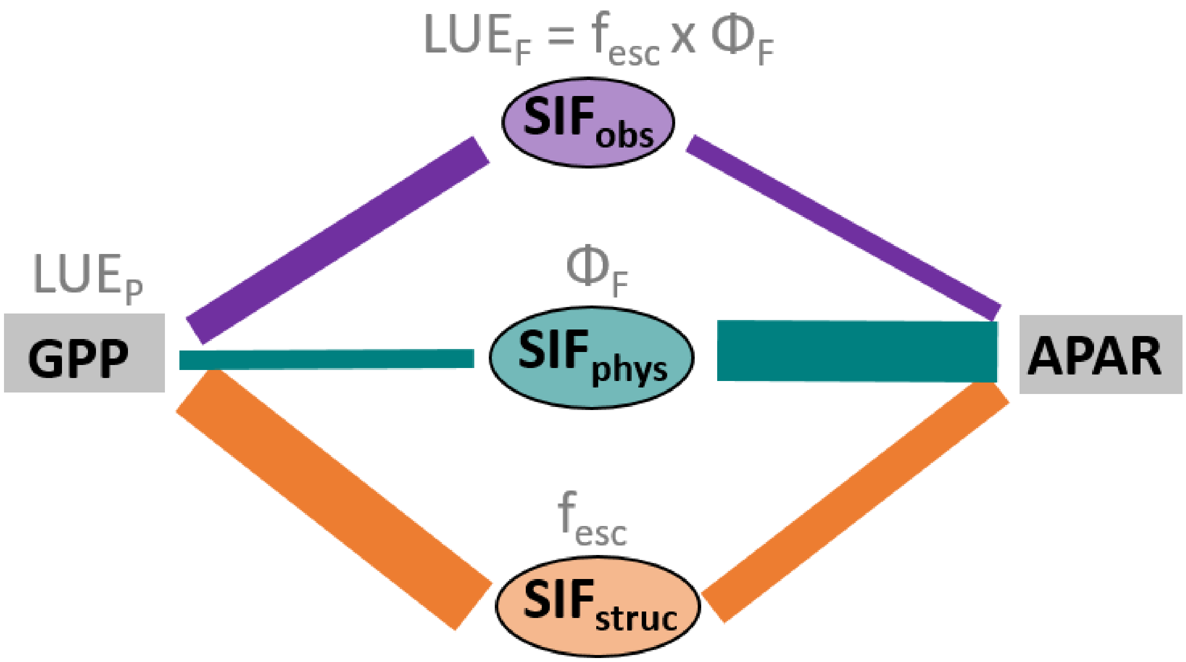

Figure 8: Schematic overview of the observed relationships between SIF -related terms and either absorbed photosynthetically active radiation ($APAR$) or gross primary productivity (GPP). The relationships of canopy-level observed SIF (SIF_{obs}) and its two components, namely the physiological part (SIF_{phys} =SIF_{obs} /f_{esc}) and its structural part (SIF_{struc} =SIF_{obs} /Φ_F) are shown. In addition to the flux terms that all contain $APAR$ as main driver, also the corresponding efficiency terms are indicated in grey color on top of the flux variables. LUE_P is the photosynthetic light use efficiency, LUE_F the apparent light use efficiency of SIF_{obs} (LUE_F= SIF_{obs} /$APAR$), f_{esc} is the escape fraction and Φ_F is the physiological SIF yield. The line widths between flux terms represent strength of linear correlations (not to scale) based on the results of half-hourly time series at the seasonal time scale. Seasonal consistency of slope values is also taken into account in the line widths.

When examining our results in more detail for rice and corn when including seasonal variability, we found strict agreement with the different Cases of improvement or degradation in relationships to GPP of SIF_{struc} or SIF_{phys} compared to SIF_{obs} laid out in Table 2. These datasets strongly satisfied both Case 4 (SIF_{struc}>SIF_{obs} for GPP, f_{esc} strongly correlated to LUE_P) and Case 6 (SIF_{phys}<SIF_{obs} for GPP, Φ_F uncorrelated to LUE_P), offering strong evidence in support of H_{struc} (Table 4). In particular, the correlation of f_{esc} to LUE_P was considerably strong ($0.3 \le R^2 \le 0.6$), while the correlation of Φ_F to LUE_P was weak in all cases (R^2 < 0.1;Figs. 5-7).

For the diurnal variability of rice and corn, we found our results corresponded to Case combinations that did not clearly support either H_{struc} or H_{phys} as one Case (4) was associated with one hypothesis and another Case (1; SIF_{phys}>SIF_{obs} for GPP, f_{esc} strongly related to Φ_F) with the other hypothesis (Tables 2, 4). However, the results partly supporting H_{phys} were weaker than those partly supporting H_{struc} (Figs. 4, 7). Moreover, when comparing the performance of GPP estimation of SIF_{struc} and SIF_{phys} to $APAR$ rather than SIF_{obs} as reference, we found that, actually, neither SIF_{struc} nor SIF_{phys} improved over $APAR$ (Fig. S6). In fact, SIF_{phys} perfomed considerably worse than $APAR$ while SIF_{struc} had similar performance as $APAR$ for corn and slightly worse performance than $APAR$ for rice (Fig. S6a,c). The worse performance of SIF_{struc} compared to $APAR$ for diurnal GPP estimation might appear surprising given the moderate correlation of f_{esc} to LUE_P (Fig. 7b) but this could be explained by seasonally varying slopes of the diurnal relationships resulting in no improvement or slight degradation at the seasonal time scale. In any case, the diurnal variability results were somewhat inconclusive and neither strongly supporting H_{phys} nor H_{struc}.

The wheat dataset offered mixed evidence in partial support of both H_{struc} and H_{phys} (Table 4). Nevertheless, the seasonal correlation of f_{esc} to LUE_P was considerably stronger than the correlation of Φ_F to LUE_P (R^2 values of 0.61 and 0.24, respectively) and the same pattern held for the corresponding flux relationships of SIF_{phys} vs. SIF_{struc} for GPP estimation (Figs. S5 a,c and 7a,b). Our findings therefore appear to support a weaker form of H_{struc} for wheat at the seasonal time scale.

In terms of Cases, only the seasonal+diurnal variability results of wheat came somewhat close to fully supporting H_{struc} for wheat. Case 6 satisfied by both flux and efficiency results but Case 4 only by the efficiency results (Table 4). The absence of improvement of SIF_{struc} over SIF_{obs} for GPP estimation despite improvement for $APAR$ estimation (Table 2) was consistent in all variability cases (Table 4). For the sake of convenicne, we attributed such intermediary results to a Case "X" in Table 4, which was not addressed in Table 2, and appears to be inconsistent with the framework at first sight. The results corresponding to Case X can be understood, however, when taking into account the strong correlations of f_{esc} to LUE_F as well as the moderate correlation of f_{esc} to Φ_F at the seasonal time scale (Fig. S4). Such a correlation of f_{esc} and Φ_F is consistent with the existence of coordination of canopy structure and leaf physiology (Badgley et al., 2019, 2017). For the diurnal and seasonal variability efficiency results, the same Case combination as for diurnal results of rice and corn (4, 1) were satisfied (Table 4), indicating partial support for H_{struc} and H_{phys}.

The diurnal results of wheat are noteworthy in several respects. First, f_{esc} and Φ_F showed similar levels of correlation to LUE_P (Fig. 7a,b). Second, LUE_F was slightly more strongly correlated to LUE_P than either Φ_F or f_{esc} (Fig. S5b). Third, wheat was the only dataset where the diurnal correlation to

GPP of any of the three SIF variables outperformed $APAR$ (Fig. S6a-c). However, this improvement was small in absolute terms (ΔR^2<0.05).

Table 4: Overview of evaluation of results in terms of agreement with different cases as listed in Table 2 and support for the corresponding hypotheses. The pair of case numbers for performance of the structural component of SIF (SIF_{struc}) and the physiological component of SIF (SIF_{struc}) compared with observed canopy-level SIF (SIF_{obs}) is given in the 'fluxes' columns for each crop dataset. Similarly, the pair of case numbers for the relationships to photosynthetic light use efficiency (LUE_P) and degree of variability of the escape fraction (f_{esc}) and the physiological SIF yield (Φ_F) is given in the 'efficiencies' column. Case 'X' refers to a case that was not listed in Table 2 showing no clear increase in GPP estimation performance of SIF_{struc} over SIF_{obs} while showing improvement for APAR estimation. The overall conclusion for the support of the main hypotheses is given in the bottom row. Results that are not strictly consistent with the hypothesis H_{struc} are highlighted in bold.

Variability	**Rice**		**Wheat**		**Corn**	
	Fluxes	Efficiencies	Fluxes	Efficiencies	Fluxes	Efficiencies
Seasonal	(4, 6)	(4, 6)	(**X**, 6)	(4, **1**)	(4, 6)	(4, 6)
Seasonal + diurnal	(4, 6)	(4, 6)	(**X**, 6)	(4, 6)	(4, 6)	(4, 6)
Diurnal	(4, **1**)	(4, **1**)	(**X**, 6)	(4, **1**)	(4, **1**)	(4, **1**)
Conclusion for Seasonal scale	-> H_{struc}		**->** H_{struc} **(**H_{phys}**)**		-> H_{struc}	
Conclusion for diurnal scale	-> neither		-> neither		-> neither	

4.2 f_{esc} , SIF_{struc} and the important role of NIR_V

We found strong evidence of the considerable seasonal dynamics in f_{esc} that corresponded with seasonal variations in LUE_P (Figs. 5 and 7). The strong variation of f_{esc} is consistent with previous studies using both process-based simulations and in situ observations (Du et al., 2017; Fournier et al., 2012; Yang and van der Tol, 2018; Zeng et al., 2019) and contradicts studies assuming constant f_{esc} (e.g. Guanter et al., 2014). While there was also diurnal variation of f_{esc} (Fig. 7), it was considerably smaller than the seasonal component. The diurnal variation of f_{esc} could be caused by interactions of canopy structure with changing solar zenith angle as well as by leaf movements (Goulas et al., 2017).

We believe our study is the first one that explicitly investigated the relationships of f_{esc} to canopy $\mathrm{LUE_P}$, which makes a comparison with other literature somewhat indirect. Nevertheless, a strong link to previous studies on the NIR_V-GPP relationship (Badgley et al., 2019, 2017) can be established in two different ways. First, SIF_{struc} is calculated as the simple product of NIR_V and PAR (Table 1). Therefore, our results can be considered an extension of the NIR_V-GPP relationship first identified by Badgley et al. (2017) to the sub-daily scale. Indeed, we could demonstrate that the GPP estimation performance of the product of NIR_V times PAR (NIR_VP) converges to NIR_V at time scales of about two weeks (Fig. S7). It is noteworthy that in contrast to other studies that simply multiplied NIR_V by PAR or short wave radiation without a solid mechanistic basis (e.g. Joiner et al., 2018), we found that NIR_VP quite naturally emerges from Eqns. 3 and 5 as an estimate for SIF_{struc} (Table 2). Second, under certain conditions, NIR_V can be considered as a proxy of f_{esc}, as f_{esc} can be estimated as fraction of NIR_V over $fPAR$ (Eqn. 3). Thus, in cases where $fPAR$ approaches one (e.g., at the peak of the growing season) or, more generally, when fPAR is is not varying much in a certain temporal period or spatial area, the fraction of NIR_V over $fPAR$ will converge to NIR_V in terms of variability. This perspective might be relevant for applications in dense tropical forests, where $fPAR$ is very high and has little variations.

Apart from these two ways of linking our results to NIR_V, it is instructive to consider Eqn. 3 for reinterpreting NIR_V in terms of its mechanistic meaning. More specifically, Eqn. 3 can be rearranged to read $NIR_V = fPAR \cdot f_{esc}$, implying that NIR_V integrates light absorption and f_{esc}. This is an intriguing consequence of the findings of Zeng et al. (2019) given that the relationship of NIR_V to GPP was originally only empirically motivated. . Our results add further nuance by establishing an empirical relationship between f_{esc} and LUE_P.

A point of practical interest is that the product of NDVI times the upwelling NIR radiance ($NIR_V R$) shows very strong correlation to $NIR_V P$ and is therefore an alternative that only needs data from the RED and NIR bands (Appendix B). The results of $NIR_V R$ and $NIR_V P$ showed similar levels of performance for GPP estimation (Fig. B2). As $NIR_V R$ does not require separate PAR data, it might have advantages over NIR_VP for satellite-based applications at large scales where PAR data are not readily available despite recent progress (Ryu et al., 2018). At the very least, using NIR radiance, as opposed to reflectance, eliminates uncertainties that arise from translating measurements of radiance at the surface to reflectance.

Another relevant aspect of our findings is that the SIF_{struc}-SIF_{obs} relationship was more consistent than the SIF_{phys}-SIF_{obs} relationship (Fig. S8). This is due to the strong seasonality of f_{esc} and overall seasonal stability of Φ_F (Fig. 5). As f_{esc} is the slope in the $SIF_{obs} - SIF_{phys}$ relationship (assuming zero intercept), the seasonal variation of f_{esc} translates into seasonally varying slopes in the$SIF_{obs} - SIF_{phys}$ relationship, similar to the the SIF_{struc}-$APAR$ relationship (Appendix A). The SIF_{obs}-SIF_{struc} relationship, in contrast has a seasonally stable slope. The relative invariance of Φ_F when compared to f_{esc} found across all three datasets helps explain the basis of the globally consistent relationship between SIF_{obs} and NIR_V identified by Badgley, Field and Berry (2017) at the monthly time scale.

An important implication of the strong relationship of SIF_{struc} and SIF_{obs} is that SIF_{struc} is expected to exhibit characteristics similar to SIF_{obs} concerning the responses to stress. For long term stress, several studies reported good performance of satellite-based SIF_{obs} retrievals in tracking large spatial and temporal scale drought effects on both natural and agricultural vegetation (Sun et al., 2015; Wang et al., 2016; Yoshida et al., 2015). On the monthly time scales investigated in these studies, however, the main effect of drought on photosynthesis likely relates to changes in canopy structure, in particular via $fPAR$ and/or f_{esc}. Therefore, NIR_V or SIF_{struc} are expected to also capture the main response to stress at that time scale but the studies in question did not include such analyses. For short-term heat and drought conditions, however, SIF_{struc} is expected to also have limited potential to track reductions in GPP, as reported in several existing studies of SIF_{obs} (Wieneke et al., 2018; Wohlfahrt et al., 2018). This is not surprising as a time scale of one to two weeks is too short to significantly alter most canopy structural traits, such as LAI, or leaf biochemical traits, such as chlorophyll content, although leaf angles might change more rapidly. As our crop datasets did not include strong heat or drought stress, however, we could not investigate the responses to short- and long-term stresses.

One case where the strong relationship between SIF_{struc} and SIF_{obs} is expected to break down is in evergreen needle leaf forests (ENF), as they are a special case with seasonally very stable canopy structure apart from changes in the understory and branch growth. Even more importantly, it is known that in ENF there is a pronounced seasonal cycle of Φ_F due to sustained non-photochemical quenching in winter winter (Porcar-Castell, 2011; Porcar-Castell et al., 2014; Raczka et al., 2019). SIF_{struc} is therefore expected to also have limitations for GPP estimation in ENF ecosystems as canopy structure is rather stable but GPP shows very similar seasonal variations as SIF_{obs} (Magney et al., 2019). Despite all these differences in canopy structure variability, however, Badgley, Field and Berry (2017) found strong correlations of monthly NIR_V to GPP at the global scale including ENF data. This could potentially be explained by the typically low PAR values in winter that coincide with low LUE_P at high latitudes where most of ENF ecosystems are located.

4.3 Φ_F and SIF_{phys}

While we found that variability of Φ_F, measured in terms of the coefficient of variation (CV), were similar to that of f_{esc} (Fig. 7), the variability of Φ_F did not correlate with LUE_P for rice and corn. In fact, for these two crops, the considerably high seasonal CV of Φ_F appeared to be mainly caused by fluctuations around the mean value without a clear seasonal trend (Fig. S3). This was not the case for wheat, however, which showed more stable values and a clearly decreasing trend coinciding with senescence as well as a weak level of correlation (Figs. 5, 7, and S2). We think that this difference between datasets might be partly explained by the better signal quality of SIF_{obs} in the wheat dataset, which is likely related to the much higher acquisition frequency (Table 3; see Section 4.4 for a more detailed discussion). Nevertheless, our results seem consistent with known, leaf-level patterns of small variation of Φ_F at diurnal (Gu et al., 2019) and seasonal time scales (Goulas et al., 2017). Moreover, Goulas et al. (2017) only found a weak correlation between actively measured Φ_F and LUE_P at the leaf level, which is consistent with our canopy-level findings (Figs. 5, 6, 7). At the canopy level, previous studies that have shown a stronger SIF_{obs}-$APAR$ than SIF_{obs}-GPP relationship, can similarly be interpreted as indirect evidence of Φ_F having little variation over the course of the growing season (Miao et al., 2018; Wieneke et al., 2018; K. Yang et al., 2018; Yang et al., 2015).

We found consistently better $APAR$ estimation performance of SIF_{phys} compared to SIF_{obs} (Figs. 3 and 4). Liu et al. (2018) previously reported similar results based on site data and airborne images. However, when comparing site-level results, there were some differences between our studies. While our study was based on continuous and long-term data and we found improvements in the relationship to $APAR$ for all sites separately, the site-level results of Liu et al. (2018) were based on very limited data for each site (1-5 days) and showed the strongest improvement for the combined analysis of all three datasets. The absence of improvements of SIF_{phys} over SIF_{obs} for $APAR$ estimation for the separate analyzes of two of the three sites in Liu et al. (2018) could be explained by the use of data from single measurement days where only the diurnal variation of f_{esc} plays a role, which is considerably weaker than the seasonal variation covered in our datasets (Fig. 7d). Although in our results SIF_{struc} had similarly high R^2 values for $APAR$ estimation as SIF_{phys}, SIF_{phys} had the more consistent relationships in terms of seasonal slope stability (Appendix A).

It is with a certain irony that we conclude from our analyses that, SIF_{phys}, the physiological component of SIF_{obs}, appears to be better suited for estimating $APAR$ as opposed to estimating GPP (Figs. 3, 4, A1). This conclusion is in stark contrast to the widely held hopes of the SIF community to use the inherent physiological link between chlorophyll fluorescence and photosynthesis for improved GPP estimation (see, for example, Porcar-Castell et al., 2014). Although Φ_F and SIF_{phys} should theoretically help explain short-term variations in LUE_P and GPP due to changes in non-photochemical quenching, such effects were not observed in the data we analyzed. Such possibilities, as well as the prospect of using SIF_{phys} as the basis for consistently estimating $APAR$ at the global scale (e.g., Ryu et al., 2018, 2019), deserve continued attention in future research. Logically speaking, however, using SIF_{phys} for $APAR$ estimation is a somewhat circular approach as $fPAR$ is used in the calculation of f_{esc} that is needed to estimate SIF_{phys} (Table 1). Approaches to circumvent this circularity, e.g. iterative methods starting from existing $fPAR$ products, would therefore be needed.

4.4 Main sources of uncertainties and potential effects on our results

We are aware that despite our efforts in data collection and analysis, there are several limitations potentially affecting our results. These include a footprint mismatch between SIF and eddy covariance observations, noise and bias in the SIF retrieval, and the use of total $fPAR$ ($fPAR_{tot}$) rather than green $fPAR$ ($fPAR_{green}$). These aspects are discussed in more detail below.

Within the footprint of an eddy covariance tower, there might be considerable spatial heterogeneity in canopy structure and overall GPP. However, the radiometric footprint of the instruments used for SIF_{obs} retrieval and NIR_V observations is typically much smaller than the eddy covariance footprint, meaning the remote measurements typically do not fully capture the effects of spatial heterogeneity in canopy-level fluxes (Gamon, 2015; Marcolla and Cescatti, 2017). While crop fields tend to be more homogeneous than natural ecosystems, this factor is still expected to affect our results to some degree. There were clear differences in the areas of the radiometric footprints in our datasets (Table 3), with the rice paddy instruments covering a much larger area despite lower height above canopy due to the use of the bihemispheric viewing geometry (Liu et al., 2018; Marcolla and Cescatti, 2017). However, the effect on the results depends on several other factors such as the degree of heterogeneity in the footprint and is therefore hard to quantify. In any case, efforts should be made for covering larger areas of the eddy flux tower footprints with hyperspectral sensors to minimize footprint mismatch effects.

The retrieval of SIF_{obs} introduces additional uncertainties (noise and bias), largely arising from the difficulty of retrieving the small SIF signal (~1% of the absorbed light) from the much stronger background of reflected sunlight (Damm et al., 2011; Frankenberg and Berry, 2018; Meroni et al., 2009). In particular, these uncertainties quite directly propagate into uncertainties in our estimates of Φ_F, as Φ_F was calculated as the 'residual' of SIF_{obs} and SIF_{struc}, assuming that SIF_{struc} can is much less affected by measurement uncertainties. The reason for this assumption is that only direct observations of RED and NIR reflectance and PAR were used to calculate SIF_{struc} (Table 1). A similar reasoning as that for Φ_F is valid for SIF_{phys} as the latter is the product of Φ_F times $APAR$.

Apart from different choices of SIF_{obs} retrieval algorithms in interaction with the spectral and radiometric characteristics of the instruments and processing (Table 3, Section 2.2), differences in uncertainty in SIF_{obs} between datasets also arises from considerable differences in the number of spectra collected per minute. In particular, the wheat site typically collected about 60-120 times the number of spectra measured at the rice and corn sites (Table 3). Such a high acquisition frequency translates into stronger noise reduction in SIF retrievals via temporal averaging. We found that, based on theoretical considerations, this noise reduction effect via temporal averaging was not yet saturated for 30 min averages and 1 Hz sampling frequency (results not shown), indicating a considerable effect on improving the signal quality for the wheat dataset compared to rice and corn, given that the wheat site also used optimized integration time values.

Based on the above considerations and the potentially large impact of SIF uncertainties on our results, we used the SCOPE model (van der Tol et al., 2009; van der Tol et al., 2014; Vilfan et al., 2016) in an attempt to quantify such effects for the example of rice (Supplementary Text S1, Fig. S10). We found that SCOPE results without noise showed considerably stronger correlation of Φ_F to LUE_P and notably weaker correlation of f_{esc} to LUE_P than in our results (Fig. S10). When adding random noise to half-hourly output at both diurnal and seasonal time scales with a magnitude based on an attempt to match the CV of observations (Text S1, Fig. S9), we could mostly match the relative patterns of correlations of Φ_F and LUE_F to LUE_P observed for rice, while the discrepancies for the f_{esc} -LUE_P correlation remained (Fig. S10). In particular, the results supported the interpretation of the higher correlation of Φ_F to LUE_P in the wheat data being a direct byproduct of less noise contamination in retrievals of SIF_{obs} (Figs. 5, 6, and 7). Only by adding the random noise at both diurnal and seasonal time scales could we reproduce the observed patterns, indicating that, for SIF retrieval, different noise and bias characteristics on multiple time scales may play an important role. Overall, our simulation results underline the importance of improving SIF_{obs} signal quality by e.g. increasing acquisition frequency to reduce retrieval noise.

We think the uncertainties related to SIF retrieval do not affect our main conclusions in their essence. First, the strong evidence for H_{struc} is not affected by this aspect at all, as SIF_{struc} and f_{esc}

are not based on SIF_{obs} retrievals but on NIR_V (Table 1). Second, although the lack of evidence supporting H_{phys} appears to be partly caused by noise issues, even the wheat dataset, which apparently had the best SIF_{obs} quality, did not show indications of better performance of physiological over structural information. This might be partly caused by footprint mismatch issues and other uncertainties related to GPP observations, but it still implies that there may be severe practical limitations of extracting relevant physiological information from SIF_{obs}. As our results suggests that this holds even for the site level, it is likely to be even more challenging for large scale airborne or satellite-based applications, although other aspects also come into play when investigating spatial relationships (see Section 4.5). Another potential explanation for part of the discrepancy between observations and SCOPE results could be limitations in the SCOPE model itself that uses a leaf-fluorescence submodel that is based on a limited dataset (van der Tol et al., 2014).

Apart from the analysis of SIF_{obs} retrieval noise effects, we also used the SCOPE simulation output to assess the uncertainties related to applying Eqn. 3 to estimate Φ_F from SIF_{obs} (Table 1). We found that even without adding noise to the SIF_{obs} output, the uncertainty in estimated f_{esc} had a considerable effect on Φ_F estimation (Fig. S11), which indicates the high sensitivity of Φ_F estimation to f_{esc} estimation errors. Therefore, refining the f_{esc} estimation by improving the corrections for the NDVI values of soil (Zeng et al., 2019) is expected to have a notable impact on Φ_F estimation results. However, the simulated effects of SIF_{obs} retrieval noise strongly dominated over the uncertainty introduced by the Φ_F estimation method based on Eqn. 3 (Figs. S11c,d).

It is also worth noting that we used field observations of $fPAR_{tot}$ rather than $fPAR_{green}$ that only captures the light absorbed by chlorophyll. Previous studies have suggested to use the fraction of green LAI to total LAI to estimate $fPAR_{green}$ from $fPAR_{tot}$ (Gitelson et al., 2018; Gitelson and Gamon, 2015). Such data were only available for the rice dataset, however, preventing a consistent application of the $fPAR_{green}$ approach to all datasets. Nevertheless, we think that using in situ measured $fPAR$ has advantages over using an indirect estimate based on canopy reflectance due to the uncertainties in the latter approach. Using $fPAR_{tot}$ rather than $fPAR_{green}$ is expected have an impact mainly during the senescence phase at the end of the growing season and logically should affect both the estimates of f_{esc}, and SIF_{phys} (Table 1). As Φ_F was estimated via SIF_{obs} /SIF_{struc} (Table 1), however, and SIF_{struc} was estimated as NIR_V x PAR, the estimations of Φ_F and SIF_{struc} were not affected by this issue. Therefore, the interpretation of results and conclusions, especially the strong performance of SIF_{struc} for GPP estimation is not substantially affected by using $fPAR_{tot}$.

4.5 Implications for large scale SIF-based GPP estimation

Ultimately, the main motivation to study SIF-GPP relationships is to improve the remote and large-scale estimation of GPP (Ryu et al., 2019). We found that the structural component of SIF (SIF_{struc}) showed strong linear relationships to GPP that were as good as or even better than those based on SIF_{obs}. However, our results strongly focused on crops, the site level and short time scales. Furthermore, our analysis was conducted for all three sites separately and thus strongly focused on temporal variability.

Large scale applications using satellite SIF retrievals, however, tend to capture variations across space more than variations in time. Even when longer time series of SIF are considered, the number of pixels across space is typically much larger than the number of observation time steps. Therefore, we need to be cautious in making incorrect generalizations from the temporal case to the spatial case. In particular, several global scale studies (spatial case) have shown differences in the slope of SIF_{obs}-GPP relationships between ecosystems (Guanter et al., 2014; Sun et al., 2018; Yongguang Zhang et al., 2016). Since the main origin of the slope differences for a given photosynthetic pathway is strongly suspected to be f_{esc} (Zeng et al., 2019), SIF_{struc} should show essentially the same tendencies as SIF_{obs}. Therefore, using f_{esc} to normalize the differences in slope between SIF_{obs} and GPP in different ecosystems, is expected to improve spatial SIF-GPP relationships. Judging from our results, however, the improvement in spatial patterns goes together with a degradation of temporal relationships, though this has a small effect when spatial patterns are dominant in the data considered.

For SIF_{struc}, the approach of using f_{esc} to correct for slope differences between SIF_{obs} and GPP is 1) not possible as NIR_V is already used to calculate SIF_{struc} and 2) not desirable as f_{esc} contains the $\mathrm{LUE_P}$-relevant information in addition to $APAR$. It seems, therefore, that for SIF_{struc}-based GPP estimation, an ecosystem-dependent slope has to be applied as was partly done in Badgley et al. (2019). This is particularly relevant for evergreen needleleaf forests (ENF) that have a much lower NIR reflectance despite rather high GPP during the growing period, as can be inferred also from previous studies investigating SIF_{obs} -GPP relationships (Sun et al., 2018; Yao Zhang et al., 2018a). Based on our results, different slopes need to be applied for C3 and C4 species no matter if SIF_{obs} or SIF_{struc} is used (Fig. S12), which indicates that ecosystem- or pathway-dependent slopes will be required to some degree for global studies in any case. Further research is needed to determine if SIF_{obs} considerably outperfors SIF_{struc} for GPP estimation in ENF ecosystems as suggested by Magney et al. (2019). If so, it is likely worth testing whether using the chlorophyll/carotenoid index, CCI, (Gamon et al., 2016) or PRI (Gamon et al., 1992; Wong and Gamon, 2015a, 2015b) to estimate GPP in ENF and reserving the use of with SIF_{struc} into estimate GPP for all other ecosystems yields comparable or better performance than SIF_{obs} at the global scale.

Apart from the different impacts of temporal and spatial variation, there is another aspect to consider for satellite applications. In contrast to ground-based observations, non-geostationary satellites take snapshots at a given moment in time, not daily mean values. While the expected effects of this were previously simulated and directly examined in several studies (Yongguang Zhang et al., 2016; Yao Zhang et al., 2018b), we found overall consistent patterns compared to using half-hourly values with only minor differences (results not shown). We therefore conclude that our findings are particularly relevant for satellite-based applications when considering the temporal (per-pixel) variability. Future SIF retrievals from geostationary missions such as TEMPO (Zoogman et al., 2017) or GeoCarb (Moore III et al., 2018) could provide the basis for large scale analyses similar to our site-level approach.

5. Conclusion

We mechanistically decomposed canopy-level SIF_{obs} at three crop sites into its physiological and structural components and examined their relationships to GPP and $APAR$. We found that the structural component of SIF, was a better estimator of GPP than the physiological component of SIF and even outperformed SIF_{obs} for GPP estimation for two of the three sites and comparable performance to SIF_{obs} for the remaining crop. The better performance of the structural component of SIF was explained by the considerable seasonal correlation of the escape fraction f_{esc} to the photosynthetic light use efficiency LUE_P across the three sites. The physiological component of SIF, in contrast, improved the relationship to $APAR$ compared to SIF_{obs}, but had a considerably weaker performance for GPP estimation than SIF_{obs}. The latter could be explained by the absence of clear seasonal patterns in Φ_F, which also explains the stronger relationship of SIF_{phys} to $APAR$. Even at the diurnal scale, Φ_F did not outperform f_{esc} in terms of correlation to LUE_P except in the case of the wheat site. The structural component of SIF can be observed on the basis of the near-infrared reflectance of vegetation NIR_V with multispectral instruments without the need for SIF retrieval or explicit $fPAR$ information. Complementary PAR information can be obtained from other sensors or the upwelling near-infrared radiance of vegetation can be used directly.

Our findings focus on the temporal relationships at half-hourly resolution and the seasonal time scale and highlight the importance of the canopy structure effects on the SIF_{obs} signal, as well as SIF_{struc} as effective GPP proxy in crops. Apart from providing further evidence of the practical usefulness of NIR_V in general and the NIR_V-based escape fraction formula in particular, we presented a comprehensive framework of analyzing the separate contributions of Φ_F and f_{esc} that is expected to stimulate future research.

Acknowledgements

Many people contributed to the collection and processing of the in situ data sets and we are grateful for their contributions. We thank Kaige Yang, Hyungsuk Kimm and Jongmin Kim from Seoul National University (SNU) for contributing to field measurements and SIF retrieval processing for the rice paddy data set. We also thank other member of the group at SNU for contributing to the collection of field observations such as LAI and Vcmax that were helpful for running the SCOPE simulations and interpreting the results. We also thank Ari Kornfeld from the Carnegie Institution for Science and Xi Yang from the University of Virginia for helping to set-up and run the spectrometer systems in the rice paddy and providing support in the data processing and troubleshooting. We thank Olivier Marloie for processing eddy covariance flux data for the wheat field and are grateful for the contributions of the team at Ecole Polytechnique to the development of the TriFLEX instrument that was used for the data collection. We also thank Shihua Zhu from Nanjing University as well as Hezhou Wang, Pengju Wu and other researchers from the ShangQiu station of the Farmland Irrigation Research Institute of the Chinese Academy of Agricultural Sciences for their support with field measurements for the corn data set. This research was funded by the National Research Foundation of Korea (NRF-2016M1A3A3A02018195). The SiF joint workshop between SNU and Nanjing University funded by the National Research Foundation of Korea (NRF-2018K2A9A2A05018142) contributed to this manuscript. Processing of the wheat data was funded by the Centre National d'Etudes Spatiales, Terre Océan Surfaces Continentales Atmosphère (CNES TOSCA) program. English proofread service was supported by Research Institute of Agriculture and Life Sciences in SNU.

Appendix A. Relationships between $APAR$ and SIF

As in Fig. 2 only the R^2 results for the relationships between SIF_{obs}, SIF_{struc} and SIF_{phys} and GPP are shown, we include the detailed relationships between $APAR$ on the one hand and SIF_{obs}, SIF_{struc} and SIF_{phys} on the other hand here (Fig. A1).

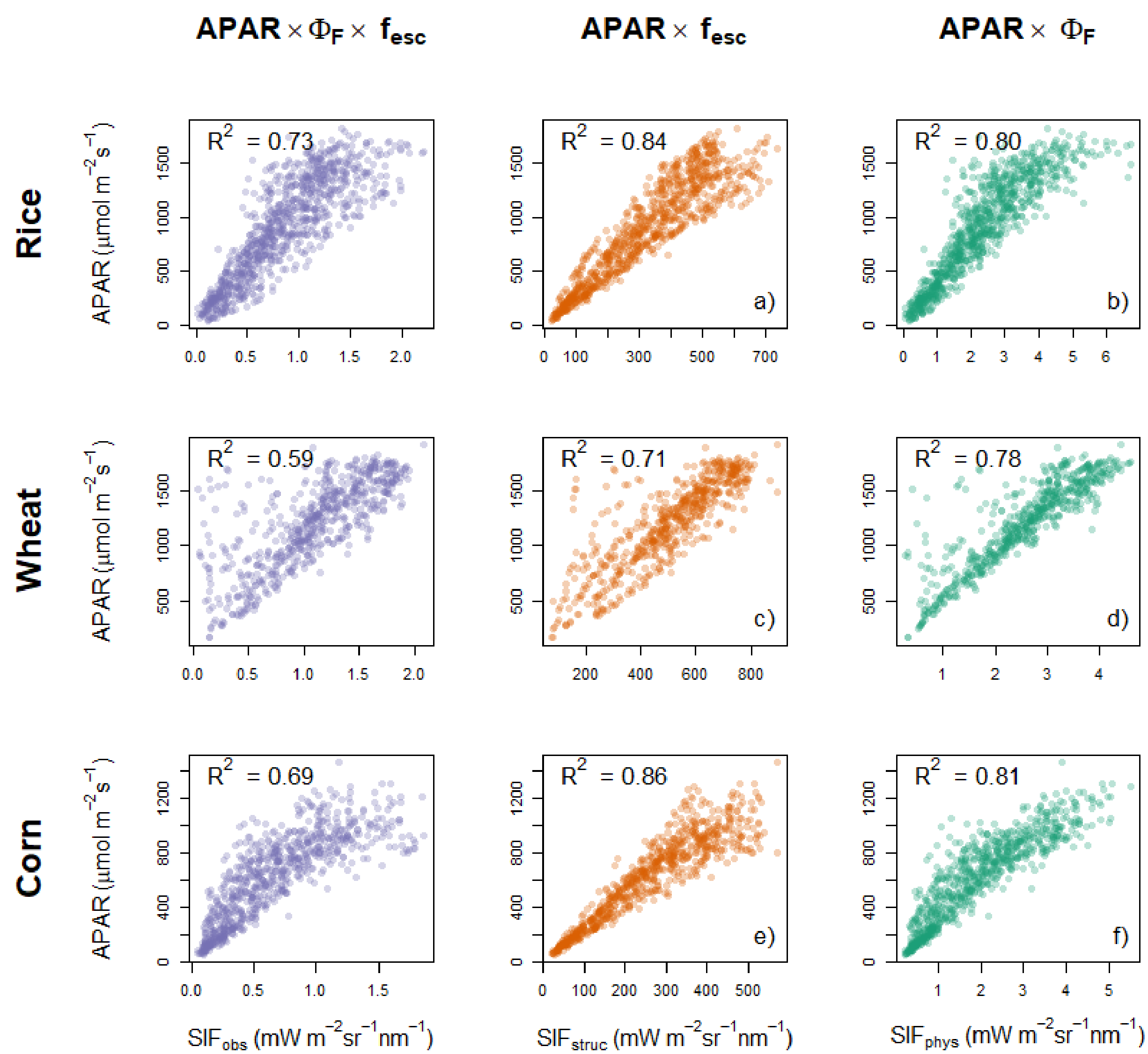

Figure A1: Illustration of the effect of seasonal changes in f_{esc} on the relationship between SIF_{struc} and $APAR$ for the <u>*wheat*</u> *dataset. As f_{esc} is the ratio of SIF_{struc} and $APAR$, its seasonal changes (panel c) directly correspond to seasonal changes of the slope in the relationship.*

It is instructive to study the patterns in the scatterplots in Fig. A1, as there are partly relatively small differences in R^2 between SIF_{phys} and SIF_{struc} but clear patterns of seasonally varying slopes in the

SIF_{struc}-$APAR$ relationships. This can be well illustrated with the example of the wheat dataset (Fig. A2). Assuming a zero intercept, the slope in the SIF_{struc}-$APAR$ relationship is simply the ratio of $APAR\ /SIF_{struc}$, which is $1/f_{esc}$. As f_{esc} is showing considerable seasonal variation, this is reflected also in the slope. An illustration of this situation is shown in Fig. A2. The reason why the SIF_{phys}-$APAR$ relationship does not show such varying slope patterns is that Φ_F did not show clear seasonal trends (Fig. 5d-f).

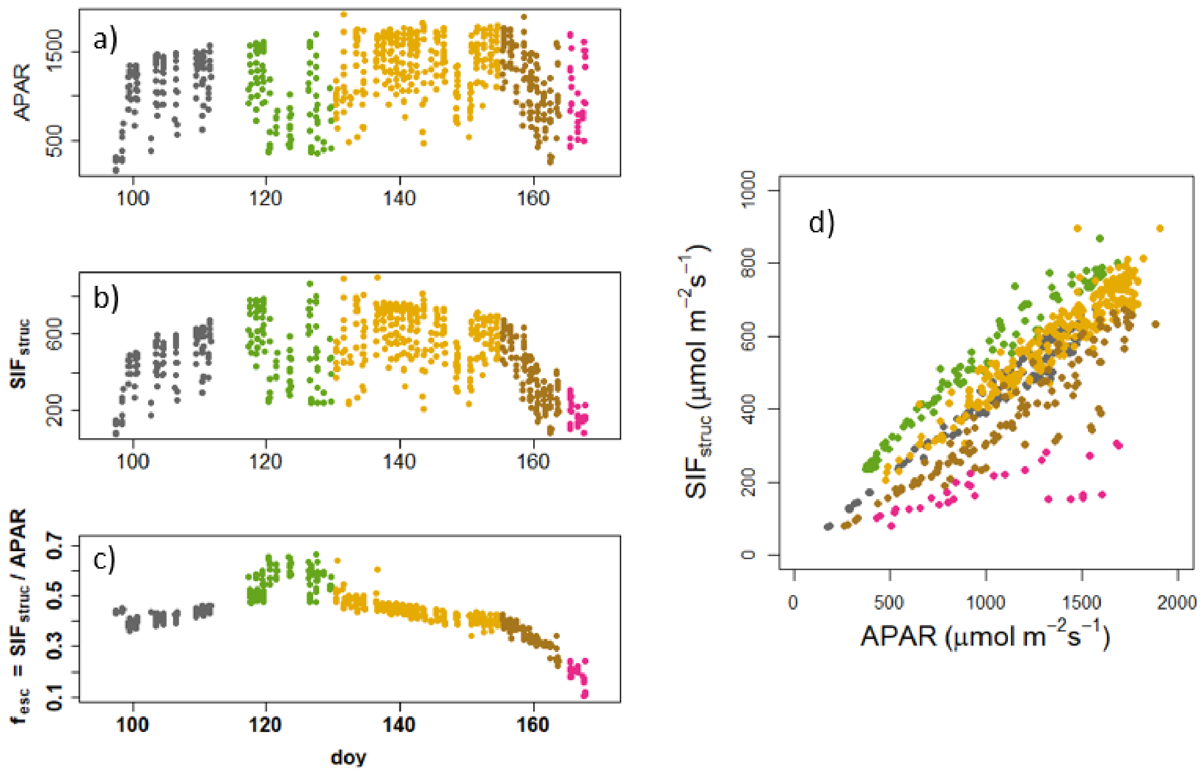

Figure A2: Illustration of the effect of seasonal changes in f_{esc}) on the relationship between SIF_{struc} and $APAR$ for the wheat dataset. As f_{esc} is the ratio of SIF_{struc} and $APAR$, its seasonal changes (panel c) directly correspond to seasonal changes of the slope in the relationship (panel d).

Appendix B. Comparison of NIR_VR and NIR_VP for practical purposes

NIR_VP = $NIR_V \cdot PAR$ requires PAR information that cannot be obtained directly from multispectral sensors designed for NDVI and NIR_V observations. Although eddy covariance towers are typically equipped with separate quantum sensors for PAR measurements, some sites without eddy covariance instruments might not have such sensors. Therefore, using the radiance version $NIR_V R$=$NIR_V \cdot (downwelling\ nir\ Radiance)$ = $NDVI \cdot (upwelling\ nir\ radiance)$ could be useful in certain circumstances ("nir" was used to denote "near-infrared" here, as "NIR" was defined as nir reflectance, see Table 2). For example, when using airborne or satellite observations, the radiance data from the sensors in the atmospheric window around the O_2A band does not require atmospheric correction and therefore has a clear practical advantage (Köhler et al., 2018; Zeng et al., 2019). For all three crop datasets, we found very strong correlations of $NIR_V R$ and $NIR_V P$ when using the full half-hourly time series (Fig. B1). The reason underlying the strong $NIR_V R$ and $NIR_V P$ correlations is the strong correlation of incoming PAR and downwelling near-infrared irradiance. While it is known from atmospheric radiative transfer theory that the relationship between the downwelling near-infrared radiance and incoming PAR is affected by the diffuse fraction of PAR, this effects seems negligible at the seasonal time scale.

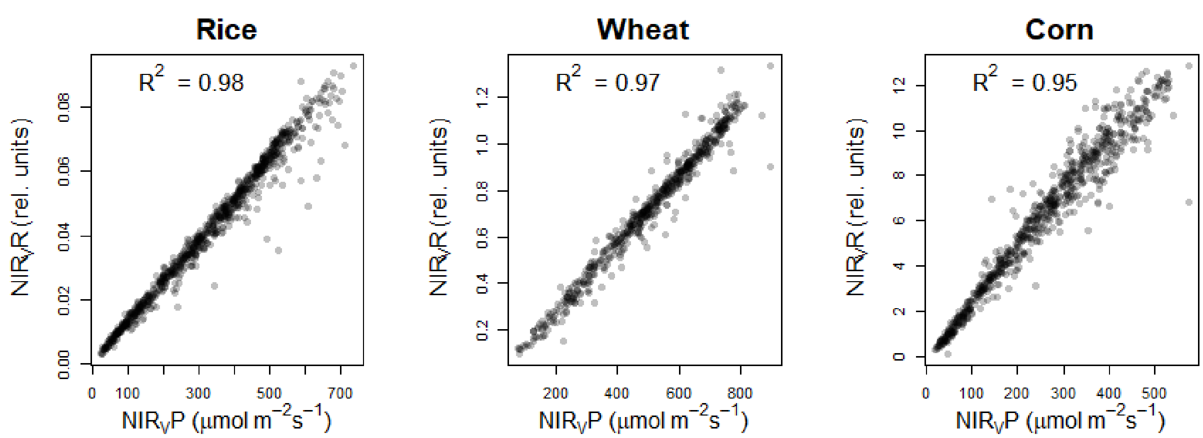

Figure B1: Comparison of $NIR_V P$ = $NIR_V \cdot PAR$ with the radiance based version $NIR_V R$ = NDVI · (near-infrared upwelling radiance) for the three crop datasets (half-hourly values, seasonal time scale). $NIR_V P$ and $NIR_V R$ are shown in relative units.

As can be expected from the very high linear correlation shown in Fig. B1, $NIR_V R$ and $NIR_V P$ have essentially the same performance for GPP estimation (Fig. B2).

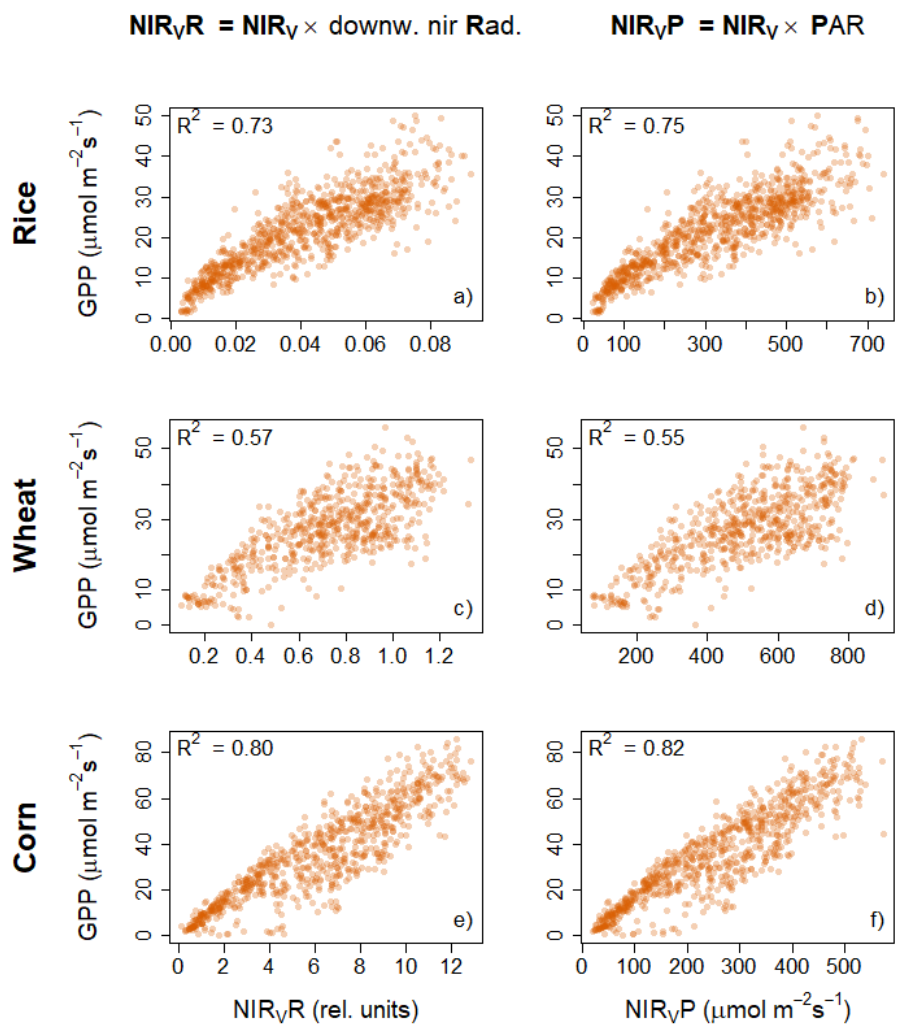

Figure B2: Relationships of a),c),e) NIR_VR to GPP compared to b),d),f) NIR_VP to GPP for the three crop datasets. Panels b),d),f) are identical to Fig. 2d,h,i) except for the x-axis label and are only shown here for easier direct comparability of results. The definitions of NIR_VR and NIR_VR is given on the top of each panel column, "downw. nir Rad." Stands for downwelling near-infrared radiance.

Appendix C. Supplementary data

Supplementary data to this article can be found online at [insert DOI link]

References

Badgley, G., Anderegg, L.D.L., Berry, J.A., Field, C.B., 2019. Terrestrial Gross Primary Production: Using NIRv to Scale from Site to Globe. Global Change Biology. https://doi.org/10.1111/gcb.14729

Badgley, G., Field, C.B., Berry, J.A., 2017. Canopy near-infrared reflectance and terrestrial photosynthesis. Science Advances 3, e1602244.

Damm, A., Erler, A., Hillen, W., Meroni, M., Schaepman, M.E., Verhoef, W., Rascher, U., 2011. Modeling the impact of spectral sensor configurations on the FLD retrieval accuracy of sun-induced chlorophyll fluorescence. Remote Sensing of Environment 115, 1882–1892. https://doi.org/10.1016/j.rse.2011.03.011

Daumard, F., Champagne, S., Fournier, A., Goulas, Y., Ounis, A., Hanocq, J.-F., Moya, I., 2010. A Field Platform for Continuous Measurement of Canopy Fluorescence. IEEE Transactions on Geoscience and Remote Sensing 48, 3358–3368. https://doi.org/10.1109/TGRS.2010.2046420

Dolman, A.J., Noilhan, J., Durand, P., Sarrat, C., Brut, A., Piguet, B., Butet, A., Jarosz, N., Brunet, Y., Loustau, D., Lamaud, E., Tolk, L., Ronda, R., Miglietta, F., Gioli, B., Magliulo, V., Esposito, M., Gerbig, C., Körner, S., Glademard, P., Ramonet, M., Ciais, P., Neininger, B., Hutjes, R.W.A., Elbers, J.A., Macatangay, R., Schrems, O., Pérez-Landa, G., Sanz, M.J., Scholz, Y., Facon, G., Ceschia, E., Beziat, P., 2006. The CarboEurope Regional Experiment Strategy. Bulletin of the American Meteorological Society 87, 1367–1380. https://doi.org/10.1175/BAMS-87-10-1367

Du, S., Liu, L., Liu, X., Hu, J., 2017. Response of Canopy Solar-Induced Chlorophyll Fluorescence to the Absorbed Photosynthetically Active Radiation Absorbed by Chlorophyll. Remote Sensing 9, 911. https://doi.org/10.3390/rs9090911

Fournier, A., Daumard, F., Champagne, S., Ounis, A., Goulas, Y., Moya, I., 2012. Effect of canopy structure on sun-induced chlorophyll fluorescence. ISPRS Journal of Photogrammetry and Remote Sensing 68, 112–120. https://doi.org/10.1016/j.isprsjprs.2012.01.003

Frankenberg, C., Berry, J., 2018. Solar Induced Chlorophyll Fluorescence: Origins, Relation to Photosynthesis and Retrieval, in: Comprehensive Remote Sensing. Elsevier, pp. 143–162. https://doi.org/10.1016/B978-0-12-409548-9.10632-3

Frankenberg, C., Fisher, J.B., Worden, J., Badgley, G., Saatchi, S.S., Lee, J.-E., Toon, G.C., Butz, A., Jung, M., Kuze, A., Yokota, T., 2011. New global observations of the terrestrial carbon cycle from GOSAT: Patterns of plant fluorescence with gross primary productivity: CHLOROPHYLL FLUORESCENCE FROM SPACE. Geophysical Research Letters 38, n/a-n/a. https://doi.org/10.1029/2011GL048738

Gamon, J.A., 2015. Reviews and Syntheses: optical sampling of the flux tower footprint. Biogeosciences 12, 4509–4523. https://doi.org/10.5194/bg-12-4509-2015

Gamon, J.A., Huemmrich, K.F., Wong, C.Y.S., Ensminger, I., Garrity, S., Hollinger, D.Y., Noormets, A., Peñuelas, J., 2016. A remotely sensed pigment index reveals photosynthetic phenology in evergreen conifers. Proceedings of the National Academy of Sciences 113, 13087–13092. https://doi.org/10.1073/pnas.1606162113

Gamon, J.A., Penuelas, J., Field, C.B., 1992. A narrow-waveband spectral index that tracks diurnal changes in photosynthetic efficiency. Remote Sensing of environment 41, 35–44.

Gitelson, A.A., Arkebauer, T.J., Suyker, A.E., 2018. Convergence of daily light use efficiency in irrigated and rainfed C3 and C4 crops. Remote Sensing of Environment 217, 30–37. https://doi.org/10.1016/j.rse.2018.08.007

Gitelson, A.A., Gamon, J.A., 2015. The need for a common basis for defining light-use efficiency: Implications for productivity estimation. Remote Sensing of Environment 156, 196–201. https://doi.org/10.1016/j.rse.2014.09.017

Goulas, Y., Fournier, A., Daumard, F., Champagne, S., Ounis, A., Marloie, O., Moya, I., 2017. Gross Primary Production of a Wheat Canopy Relates Stronger to Far Red Than to Red Solar-Induced Chlorophyll Fluorescence. Remote Sensing 9, 97. https://doi.org/10.3390/rs9010097

Gu, L., Han, J., Wood, J.D., Chang, C.Y., Sun, Y., 2019. Sun-induced Chl fluorescence and its importance for biophysical modeling of photosynthesis based on light reactions. New Phytologist. https://doi.org/10.1111/nph.15796

Guanter, L., Frankenberg, C., Dudhia, A., Lewis, P.E., Gómez-Dans, J., Kuze, A., Suto, H., Grainger, R.G., 2012. Retrieval and global assessment of terrestrial chlorophyll fluorescence from GOSAT space measurements. Remote Sensing of Environment 121, 236–251. https://doi.org/10.1016/j.rse.2012.02.006

Guanter, L., Rossini, M., Colombo, R., Meroni, M., Frankenberg, C., Lee, J.-E., Joiner, J., 2013. Using field spectroscopy to assess the potential of statistical approaches for the retrieval of sun-induced chlorophyll fluorescence from ground and space. Remote Sensing of Environment 133, 52–61. https://doi.org/10.1016/j.rse.2013.01.017

Guanter, Luis, Zhang, Yongguang, Jung, Martin, Joiner, Joanna, Voigt, M., Berry, J.A., Frankenberg, C., Huete, A.R., Zarco-Tejada, P., Lee, J.-E., Moran, M.S., Ponce-Campos, G., Beer, C., Camps-Valls, G., Buchmann, N., Gianelle, D., Klumpp, K., Cescatti, A., Baker, J.M., Griffis, T.J., 2014. Global and time-resolved monitoring of crop photosynthesis with chlorophyll fluorescence. Proceedings of the National Academy of Sciences 111, E1327–E1333. https://doi.org/10.1073/pnas.1320008111

Huang, Y., Ryu, Y., Jiang, C., Kimm, H., Kim, S., Kang, M., Shim, K., 2018. BESS-Rice: A remote sensing derived and biophysical process-based rice productivity simulation model. Agricultural and Forest Meteorology 256–257, 253–269. https://doi.org/10.1016/j.agrformet.2018.03.014

Jacquemoud, S., Baret, F., 1990. PROSPECT: A model of leaf optical properties spectra. Remote Sensing of Environment 34, 75–91.

Jacquemoud, S., Verhoef, W., Baret, F., Bacour, C., Zarco-Tejada, P.J., Asner, G.P., François, C., Ustin, S.L., 2009. PROSPECT+SAIL models: A review of use for vegetation characterization. Remote Sensing of Environment 113, S56–S66. https://doi.org/10.1016/j.rse.2008.01.026

Joiner, J., Yoshida, Y., Vasilkov, A.P., Yoshida, Y., Corp, L.A., Middleton, E.M., 2011. First observations of global and seasonal terrestrial chlorophyll fluorescence from space. Biogeosciences 8, 637–651. https://doi.org/10.5194/bg-8-637-2011

Joiner, J., Yoshida, Y., Zhang, Y., Duveiller, G., Jung, M., Lyapustin, A., Wang, Y., Tucker, C., 2018. Estimation of Terrestrial Global Gross Primary Production (GPP) with Satellite Data-Driven Models and Eddy Covariance Flux Data. Remote Sensing 10, 1346. https://doi.org/10.3390/rs10091346

Kim, J., Ryu, Y., Jiang, C., Hwang, Y., 2019. Continuous observation of vegetation canopy dynamics using an integrated low-cost, near-surface remote sensing system. Agricultural and Forest Meteorology 264, 164–177. https://doi.org/10.1016/j.agrformet.2018.09.014

Knyazikhin, Y., Schull, M.A., Stenberg, P., Mottus, M., Rautiainen, M., Yang, Y., Marshak, A., Latorre Carmona, P., Kaufmann, R.K., Lewis, P., Disney, M.I., Vanderbilt, V., Davis, A.B., Baret, F., Jacquemoud, S., Lyapustin, A., Myneni, R.B., 2013. Hyperspectral remote sensing of foliar nitrogen content. Proceedings of the National Academy of Sciences 110, E185–E192. https://doi.org/10.1073/pnas.1210196109

Köhler, P., Frankenberg, C., Magney, T.S., Guanter, L., Joiner, J., Landgraf, J., 2018. Global Retrievals of Solar-Induced Chlorophyll Fluorescence With TROPOMI: First Results and Intersensor Comparison to OCO-2. Geophysical Research Letters. https://doi.org/10.1029/2018GL079031

Kowalski, S., Sartore, M., Burlett, R., Berbigier, P., Loustau, D., 2003. The annual carbon budget of a French pine forest (Pinus pinaster) following harvest. Global Change Biology 9, 1051–1065. https://doi.org/10.1046/j.1365-2486.2003.00627.x

Li, Z., Zhang, Q., Li, J., Yang, X., Wu, Y., Zhang, Z., Wang, S., Wang, H., 2019. Solar-induced chlorophyll fluorescence and its link to canopy photosynthesis in maize from continuous ground measurements. Remote Sensing of Environment (in revision).

Liu, X., Guanter, L., Liu, L., Damm, A., Malenovský, Z., Rascher, U., Peng, D., Du, S., Gastellu-Etchegorry, J.-P., 2018. Downscaling of solar-induced chlorophyll fluorescence from canopy level to photosystem level using a random forest model. Remote Sensing of Environment. https://doi.org/10.1016/j.rse.2018.05.035

Magney, T.S., Bowling, D.R., Logan, B.A., Grossmann, K., Stutz, J., Blanken, P.D., Burns, S.P., Cheng, R., Garcia, M.A., Köhler, P., Lopez, S., Parazoo, N.C., Raczka, B., Schimel, D., Frankenberg, C., 2019. Mechanistic evidence for tracking the seasonality of photosynthesis with solar-induced fluorescence. Proceedings of the National Academy of Sciences 201900278. https://doi.org/10.1073/pnas.1900278116

Marcolla, B., Cescatti, A., 2017. Geometry of the hemispherical radiometric footprint over plant canopies. Theoretical and Applied Climatology. https://doi.org/10.1007/s00704-017-2326-z

Meroni, M., Busetto, L., Colombo, R., Guanter, L., Moreno, J., Verhoef, W., 2010. Performance of Spectral Fitting Methods for vegetation fluorescence quantification. Remote Sensing of Environment 114, 363–374. https://doi.org/10.1016/j.rse.2009.09.010

Meroni, M., Colombo, R., 2006. Leaf level detection of solar induced chlorophyll fluorescence by means of a subnanometer resolution spectroradiometer. Remote Sensing of Environment 103, 438–448. https://doi.org/10.1016/j.rse.2006.03.016

Meroni, M., Rossini, M., Guanter, L., Alonso, L., Rascher, U., Colombo, R., Moreno, J., 2009. Remote sensing of solar-induced chlorophyll fluorescence: Review of methods and applications. Remote Sensing of Environment 113, 2037–2051. https://doi.org/10.1016/j.rse.2009.05.003

Miao, G., Guan, K., Yang, X., Bernacchi, C.J., Berry, J.A., DeLucia, E.H., Wu, J., Moore, C.E., Meacham, K., Cai, Y., Peng, B., Kimm, H., Masters, M.D., 2018. Sun-Induced Chlorophyll Fluorescence, Photosynthesis, and Light Use Efficiency of a Soybean Field from Seasonally Continuous Measurements. Journal of Geophysical Research: Biogeosciences 123, 610–623. https://doi.org/10.1002/2017JG004180

Migliavacca, M., Perez-Priego, O., Rossini, M., El-Madany, T.S., Moreno, G., van der Tol, C., Rascher, U., Berninger, A., Bessenbacher, V., Burkart, A., Carrara, A., Fava, F., Guan, J.-H., Hammer, T.W., Henkel, K., Juarez-Alcalde, E., Julitta, T., Kolle, O., Martín, M.P., Musavi, T., Pacheco-Labrador, J., Pérez-Burgueño, A., Wutzler, T., Zaehle, S., Reichstein, M., 2017. Plant functional traits and canopy structure control the relationship between photosynthetic CO_2 uptake and far-red sun-induced fluorescence in a Mediterranean grassland under different nutrient availability. New Phytologist. https://doi.org/10.1111/nph.14437

Monteith, J.L., 1972. Solar Radiation and Productivity in Tropical Ecosystems. The Journal of Applied Ecology 9, 747. https://doi.org/10.2307/2401901

Monteith, J.L., Moss, C.J., 1977. Climate and the efficiency of crop production in Britain [and discussion]. Philosophical Transactions of the Royal Society of London B: Biological Sciences 281, 277–294.

Moore III, B., Crowell, S.M.R., Rayner, P.J., Kumer, J., O'Dell, C.W., O'Brien, D., Utembe, S., Polonsky, I., Schimel, D., Lemen, J., 2018. The Potential of the Geostationary Carbon Cycle Observatory (GeoCarb) to Provide Multi-scale Constraints on the Carbon Cycle in the Americas. Frontiers in Environmental Science 6. https://doi.org/10.3389/fenvs.2018.00109

Porcar-Castell, A., 2011. A high-resolution portrait of the annual dynamics of photochemical and non-photochemical quenching in needles of Pinus sylvestris. Physiologia Plantarum 143, 139–153. https://doi.org/10.1111/j.1399-3054.2011.01488.x

Porcar-Castell, A., Tyystjarvi, E., Atherton, J., van der Tol, C., Flexas, J., Pfundel, E.E., Moreno, J., Frankenberg, C., Berry, J.A., 2014. Linking chlorophyll a fluorescence to photosynthesis for remote sensing applications: mechanisms and challenges. Journal of Experimental Botany 65, 4065–4095. https://doi.org/10.1093/jxb/eru191

R Core Team, 2012. R: A language and environment for statistical computing. R Foundation for Statistical Computing, Vienna, Austria. ISBN 3-900051-07-0, URL http://www.R-project.org/.

Raczka, B., Porcar-Castell, A., Magney, T., Lee, J.E., Köhler, P., Frankenberg, C., Grossmann, K., Logan, B.A., Stutz, J., Blanken, P.D., Burns, S.P., Duarte, H., Yang, X., Lin, J.C., Bowling, D.R., 2019. Sustained Non-Photochemical Quenching Shapes the Seasonal Pattern of Solar- Induced Fluorescence at a High-Elevation Evergreen Forest. Journal of Geophysical Research: Biogeosciences. https://doi.org/10.1029/2018JG004883

Reichstein, M., Falge, E., Baldocchi, D., Papale, D., Aubinet, M., Berbigier, P., Bernhofer, C., Buchmann, N., Gilmanov, T., Granier, A., Grunwald, T., Havrankova, K., Ilvesniemi, H., Janous, D., Knohl, A., Laurila, T., Lohila, A., Loustau, D., Matteucci, G., Meyers, T., Miglietta, F., Ourcival, J.-M., Pumpanen, J., Rambal, S., Rotenberg, E., Sanz, M., Tenhunen, J., Seufert, G., Vaccari, F., Vesala, T., Yakir, D., Valentini, R., 2005. On the separation of net ecosystem exchange into assimilation and ecosystem respiration: review and improved algorithm. Global Change Biology 11, 1424–1439. https://doi.org/10.1111/j.1365-2486.2005.001002.x

Ryu, Y., Berry, J.A., Baldocchi, D.D., 2019. What is global photosynthesis? History, uncertainties and opportunities. Remote Sensing of Environment 223, 95–114. https://doi.org/10.1016/j.rse.2019.01.016

Ryu, Y., Jiang, C., Kobayashi, H., Detto, M., 2018. MODIS-derived global land products of shortwave radiation and diffuse and total photosynthetically active radiation at 5 km resolution from 2000. Remote Sensing of Environment 204, 812–825. https://doi.org/10.1016/j.rse.2017.09.021

Sun, Y., Frankenberg, C., Jung, M., Joiner, J., Guanter, L., Köhler, P., Magney, T., 2018. Overview of Solar-Induced chlorophyll Fluorescence (SIF) from the Orbiting Carbon Observatory-2: Retrieval, cross-mission comparison, and global monitoring for GPP. Remote Sensing of Environment. https://doi.org/10.1016/j.rse.2018.02.016

Sun, Y., Frankenberg, C., Wood, J.D., Schimel, D.S., Jung, M., Guanter, L., Drewry, D.T., Verma, M., Porcar-Castell, A., Griffis, T.J., Gu, L., Magney, T.S., Köhler, P., Evans, B., Yuen, K., 2017. OCO-2 advances photosynthesis observation from space via solar-induced chlorophyll fluorescence. Science 358, eaam5747. https://doi.org/10.1126/science.aam5747

Sun, Y., Fu, R., Dickinson, R., Joiner, J., Frankenberg, C., Gu, L., Xia, Y., Fernando, N., 2015. Drought onset mechanisms revealed by satellite solar-induced chlorophyll fluorescence: Insights from two contrasting extreme events: FLUORESCENCE AND DYNAMIC DROUGHT MONITOR. Journal of Geophysical Research: Biogeosciences 120, 2427–2440. https://doi.org/10.1002/2015JG003150

van der Tol, C., Verhoef, W., Timmermans, J., Verhoef, A., Su, Z., 2009. An integrated model of soil-canopy spectral radiances, photosynthesis, fluorescence, temperature and energy balance. Biogeosciences 6, 3109–3129. https://doi.org/10.5194/bg-6-3109-2009

van der Tol, C., Berry, J.A., Campbell, P.K.E., Rascher, U., 2014. Models of fluorescence and photosynthesis for interpreting measurements of solar-induced chlorophyll fluorescence. Journal of Geophysical Research: Biogeosciences 119, 2312–2327. https://doi.org/10.1002/2014JG002713

Vilfan, N., van der Tol, C., Muller, O., Rascher, U., Verhoef, W., 2016. Fluspect-B: A model for leaf fluorescence, reflectance and transmittance spectra. Remote Sensing of Environment 186, 596–615. https://doi.org/10.1016/j.rse.2016.09.017

Wang, S., Huang, C., Zhang, L., Lin, Y., Cen, Y., Wu, T., 2016. Monitoring and Assessing the 2012 Drought in the Great Plains: Analyzing Satellite-Retrieved Solar-Induced Chlorophyll Fluorescence, Drought Indices, and Gross Primary Production. Remote Sensing 8, 61. https://doi.org/10.3390/rs8020061

Wieneke, S., Ahrends, H., Damm, A., Pinto, F., Stadler, A., Rossini, M., Rascher, U., 2016. Airborne based spectroscopy of red and far-red sun-induced chlorophyll fluorescence: Implications for improved estimates of gross primary productivity. Remote Sensing of Environment 184, 654–667. https://doi.org/10.1016/j.rse.2016.07.025

Wieneke, S., Burkart, A., Cendrero-Mateo, M.P., Julitta, T., Rossini, M., Schickling, A., Schmidt, M., Rascher, U., 2018. Linking photosynthesis and sun-induced fluorescence at sub-daily to seasonal scales. Remote Sensing of Environment 219, 247–258. https://doi.org/10.1016/j.rse.2018.10.019

Wohlfahrt, G., Gerdel, K., Migliavacca, M., Rotenberg, E., Tatarinov, F., Müller, J., Hammerle, A., Julitta, T., Spielmann, F.M., Yakir, D., 2018. Sun-induced fluorescence and gross primary productivity during a heat wave. Scientific Reports 8. https://doi.org/10.1038/s41598-018-32602-z

Wong, C.Y.S., Gamon, J.A., 2015a. The photochemical reflectance index provides an optical indicator of spring photosynthetic activation in evergreen conifers. New Phytologist 206, 196–208. https://doi.org/10.1111/nph.13251

Wong, C.Y.S., Gamon, J.A., 2015b. Three causes of variation in the photochemical reflectance index (PRI) in evergreen conifers. New Phytologist 206, 187–195. https://doi.org/10.1111/nph.13159

Yang, H., Yang, X., Zhang, Y., Heskel, M.A., Lu, X., Munger, J.W., Sun, S., Tang, J., 2017. Chlorophyll fluorescence tracks seasonal variations of photosynthesis from leaf to canopy in a temperate forest. Global Change Biology 23, 2874–2886. https://doi.org/10.1111/gcb.13590

Yang, K., Ryu, Y., Dechant, B., Berry, J.A., Hwang, Y., Jiang, C., Kang, M., Kim, J., Kimm, H., Kornfeld, A., Yang, X., 2018. Sun-induced chlorophyll fluorescence is more strongly related to absorbed light than to photosynthesis at half-hourly resolution in a rice paddy. Remote Sensing of Environment 216, 658–673. https://doi.org/10.1016/j.rse.2018.07.008

Yang, P., van der Tol, C., 2018. Linking canopy scattering of far-red sun-induced chlorophyll fluorescence with reflectance. Remote Sensing of Environment 209, 456–467. https://doi.org/10.1016/j.rse.2018.02.029

Yang, X., Shi, H., Stovall, A., Guan, K., Miao, G., Zhang, Yongguang, Zhang, Yao, Xiao, X., Ryu, Y., Lee, J.-E., 2018. FluoSpec 2—An Automated Field Spectroscopy System to Monitor Canopy Solar-Induced Fluorescence 18.

Yang, X., Tang, J., Mustard, J.F., Lee, J.-E., Rossini, M., Joiner, J., Munger, J.W., Kornfeld, A., Richardson, A.D., 2015. Solar-induced chlorophyll fluorescence that correlates with canopy photosynthesis on diurnal and seasonal scales in a temperate deciduous forest: Fluorescence and photosynthesis. Geophysical Research Letters 42, 2977–2987. https://doi.org/10.1002/2015GL063201

Yoshida, Y., Joiner, J., Tucker, C., Berry, J., Lee, J.-E., Walker, G., Reichle, R., Koster, R., Lyapustin, A., Wang, Y., 2015. The 2010 Russian drought impact on satellite measurements of solar-induced chlorophyll fluorescence: Insights from modeling and comparisons with parameters derived from satellite reflectances. Remote Sensing of Environment 166, 163–177. https://doi.org/10.1016/j.rse.2015.06.008

Zeng, Y., Badgley, G., Dechant, B., Ryu, Y., Chen, M., Berry, J.A., 2019. A practical approach for estimating the escape ratio of solar-induced chlorophyll fluorescence. Remote Sensing of Environment (in press).

Zhang, Yongguang, Guanter, L., Berry, J.A., van der Tol, C., Yang, X., Tang, J., Zhang, F., 2016. Model-based analysis of the relationship between sun-induced chlorophyll fluorescence and gross primary production for remote sensing applications. Remote Sensing of Environment 187, 145–155. https://doi.org/10.1016/j.rse.2016.10.016

Zhang, Yongguang, Guanter, L., Joiner, J., Song, L., Guan, K., 2018. Spatially-explicit monitoring of crop photosynthetic capacity through the use of space-based chlorophyll fluorescence data. Remote Sensing of Environment 210, 362–374. https://doi.org/10.1016/j.rse.2018.03.031

Zhang, Yao, Joiner, J., Alemohammad, S.H., Zhou, S., Gentine, P., 2018a. A global spatially Continuous Solar Induced Fluorescence (CSIF) dataset using neural networks. Biogeosciences Discussions 1–34. https://doi.org/10.5194/bg-2018-255

Zhang, Yao, Xiao, X., Jin, C., Dong, J., Zhou, S., Wagle, P., Joiner, J., Guanter, L., Zhang, Yongguang, Zhang, G., Qin, Y., Wang, J., Moore, B., 2016. Consistency between sun-induced chlorophyll fluorescence and gross primary production of vegetation in North America. Remote Sensing of Environment 183, 154–169. https://doi.org/10.1016/j.rse.2016.05.015

Zhang, Yao, Xiao, X., Zhang, Yongguang, Wolf, S., Zhou, S., Joiner, J., Guanter, L., Verma, M., Sun, Y., Yang, X., Paul-Limoges, E., Gough, C.M., Wohlfahrt, G., Gioli, B., van der Tol, C., Yann, N., Lund, M., de Grandcourt, A., 2018b. On the relationship between sub-daily instantaneous and daily total gross primary production: Implications for interpreting satellite-based SIF retrievals. Remote Sensing of Environment 205, 276–289. https://doi.org/10.1016/j.rse.2017.12.009

Zoogman, P., Liu, X., Suleiman, R.M., Pennington, W.F., Flittner, D.E., Al-Saadi, J.A., Hilton, B.B., Nicks, D.K., Newchurch, M.J., Carr, J.L., Janz, S.J., Andraschko, M.R., Arola, A., Baker, B.D., Canova, B.P., Chan Miller, C., Cohen, R.C., Davis, J.E., Dussault, M.E., Edwards, D.P., Fishman, J., Ghulam, A., González Abad, G., Grutter, M., Herman, J.R., Houck, J., Jacob, D.J., Joiner, J., Kerridge, B.J., Kim, J., Krotkov, N.A., Lamsal, L., Li, C., Lindfors, A., Martin, R.V., McElroy, C.T., McLinden, C., Natraj, V., Neil, D.O., Nowlan, C.R., O'Sullivan, E.J., Palmer, P.I., Pierce, R.B., Pippin, M.R., Saiz-Lopez, A., Spurr, R.J.D., Szykman, J.J., Torres, O., Veefkind, J.P., Veihelmann, B., Wang, H., Wang, J., Chance, K., 2017. Tropospheric emissions: Monitoring of pollution (TEMPO). Journal of Quantitative Spectroscopy and Radiative Transfer 186, 17–39. https://doi.org/10.1016/j.jqsrt.2016.05.008